Master of Science in Mechanical Engineering
Nov 2021

Role of Damping in NVH CAE Procedures

Rahul Sharma

Faculty of Engineering, Blekinge Institute of Technology, 371 79 Karlskrona, Sweden

This thesis is submitted to the Faculty of Engineering at Blekinge Institute of Technology in partial fulfilment of the requirements for the degree of Master of Science in Mechanical Engineering. The thesis is equivalent to 20 weeks of full time studies.

The author declares that he is the sole author of this thesis and that he has not used any sources other than those listed in the bibliography and identified as references. He further declares that he has not submitted this thesis at any other institution to obtain a degree.

Contact Information:
Author(s):
Rahul Sharma
E-mail: rahulsharma.vas@gmail.com

Supervisors:
Dr. Jonathan Westlund
Senior Road NVH CAE Engineer
Volvo Car Corporation

Dr. Ola Flodén
Associate Senior Lecturer
Lund University

University advisor:
Lic. Eng. Sravan Tatipala
Department of Mechanical Engineering

Faculty of Engineering
Blekinge Institute of Technology
SE–371 79 Karlskrona, Sweden

Internet : www.bth.se
Phone : +46 455 38 50 00
Fax : +46 455 38 50 57

Abstract

Automotive manufacturers currently face a challenge with expeditious enhancement of the vibro-acoustic properties of their vehicles. A major reason for this setback is the limited design information available during initial development stages added with limited knowledge of damping within complex structures. It is now well established that CAE studies of vibration energy flow show good correlation between power flowing into trimmed body and the interior noise produced. Aim of the dissertation is to harness this "good" correlation between power input and interior noise, by learning about the changing behaviour of system in different suspension damping scenarios. It investigates how the mechanical power input to body from suspension, interior road noise produced, and their relation is affected by changing the way damping is modelled into suspension. This is being done to make stronger design decisions from NVH point of view during the concept phases of vehicle development.

The investigation is for vehicle programs during early development phases, and hence a simplified vehicle CAE model was chosen, that contains a trimmed body with cavity fluid, and wheel suspension to capture all relevant effects of varying damping. Then, a detailed flowchart of suspension and trimmed body connections was prepared to understand how power flows into the trimmed body through suspension. Using results of power flow study, the most relevant paths and their frequency ranges were identified (to reduce the number of parts in study, yet results relevant and easily extrapolatable to a larger system). Lastly, responses are analyzed for various damping cases of suspension and trimmed body.

Results obtained show a reducing trend in mechanical input power and interior noise values with increasing damping in system. Whereas, for good correlation between power and noise, a great inclination towards structural damping localized into bushings is observed compared to other damping cases. Additionally, a strong dependency of noise, active power and reactive power is observed on trimmed body and cavity fluid damping. Active power is reduced when trimmed body damping is decreased to zero, and more so when cavity fluid damping is put to zero. On the other hand, noise and reactive power have an exact opposite correlation compared to active power and noise.

These results suggest that although active mechanical input power is the cause of interior noise, their correlation starts to deteriorate with reducing damping within the system, and instead it is the reactive power that starts to correlate better at very low damping values. But, it is physically impossible to have no damping or very low damping, so a modelling of damping within suspension that provides relatively better correlation between (active) input power and noise is when structural damping is localized within connectors.

Acknowledgments

I have to start by thanking my heartfelt team of mentors - Dr. Jonathan Westlund from Volvo Cars, Dr. Ola Flodén from Lund University, and Lic. Eng. Sravan Tatipala from Blekinge Institute of Technology. They are the ones who made a huge impact in the work done in this research and for sure they deserve my deepest gratitude in this regard. This dissertation would have been impossible for me to complete without their valuable inputs.

The guidance and support I got from them during my 6 months of work at Volvo Cars improved my technical gaps in this field and enhanced my personality. Also, the facilities provided to me at the workplace accelerated the research with all my colleagues regularly motivating me at each stage.

Finally, I would also like to thank my family for supporting me morally and my friends who helped me in any way or the other.

Contents

List of Figures

List of Tables

Chapter 1

Introduction

It takes years of research and millions of kronor to produce a new car. An effectively engineered product combined with attractive marketing strategies is what makes a vehicle ¨good value for money¨ for the customers and sells moderately well in today's competitive market. One such area within vehicle engineering that holds great importance for vehicle refinement is the study of its NVH (noise, vibration and harshness) characteristics, which aims at identification and reduction of audible sound and tactile vibration experienced by passengers, and is therefore one of the most crucial cases of dynamic loading analysed for NVH performance.

Predicting the noise and vibration characteristics of a vehicle is an extremely challenging task because of its dependence on the behaviour of a large number of parts and their highly elaborate connections contributing to complicated transmission of forces within the vehicle. The structural design of a vehicle body has come to rely heavily on CAE analysis, built upon strong engineering concepts that bridge the gap between simulation and experimental results to a great extent. Whereas, the regulation of its NVH properties has traditionally been based mostly on the use of CAE supported by simplified models or evaluated using detailed numerical models and approximated parametric values. This has failed to provide highly reliable results from NVH perspective, limited the understanding of correlation between road disturbance and cabin noise, and restricted the scope of research in vehicle NVH applications. But with the growing demand of vehicle quality in today's competitive market, it has become crucial to move towards a more accurate and highly reliable simulation driven workflow, so as to get a good idea beforehand of the acoustic properties of a vehicle under development.

During the early development stages of vehicle programs, there is a lack of detailed information available on the chassis and trimmed body design, which means important decisions must be based on the chosen concepts. In order to predict the structure borne interior noise during early design phases, a key performance indicator needs to be chosen that relates cabin noise to the tire excitation by involving structure-acoustic interaction. Acoustic pressure at occupants' ears (from mic data) can be a poor indicator unless a probabilistic FRF is available for the model [2]. So, CAE procedures for vibration energy flow through the wheel suspension into vehicle body have been proposed because of their robustness and good correlation to the road noise levels [8] [4] [7]. This method is based on mechanical input power (MIP), that is an indicator based on active vibrational power input to trimmed body from suspension. However, Mechanical Input Power, is largely dependent on modelling of damping within the suspension system, that has traditionally been simplified

in vehicle CAE models. Damping has been modelled using generalized models and damping values for most materials and connectors (such as ball joints, bushings, etc.). Therefore, evaluation of a good correlation between MIP and cabin noise would be incomplete without an in-depth investigation of modelling of damping within suspension. So, the research finds its roots in milestone in this thesis would be to identify best practises of modelling of damping within vehicle CAE models.

So, the dissertation takes first steps in a new research direction at Volvo cars, wherein it is being investigated if design decisions from NVH viewpoint can be based on power input to body and the problem being attacked is the the poor knowledge of damping within suspension. Therefore, if the central problem of this thesis is solved, it can have far-fetched implications in the automotive industry in terms of better prediction of NVH characteristics of a vehicle under development by basing design decisions on MIP, and by providing a better understanding of modelling of damping within complete vehicle CAE models for vehicle NVH simulation.

1.1 Literature review

What is considered a relevant indicator to a noise and vibration problem depends on the system type, ease of solution and output required. Power input to a structure as an indicator has been associated widely with the vibro-acoustic parameters in recent years. There have been previous studies adopting power formulation for understanding the behaviour of various types of vibrating systems owing to its simplicity, and a few such have pointed out a distinct relation between power input to a car body and cabin noise produced, calculated analytically, experimentally or by simulation.

A strong correlation has been found between mechanical power input to a car body and low frequency interior noise; [2] shows high similarities between power injected with the averaged quadratic sound pressure for a physical test setup consisting of front axle and tires, tested for different elastic mounts. However, in an era where the trend is to make accurate predictions about NVH characteristics by moving towards a more reliable simulation driven workflow, researchers have become increasingly interested in estimation of road noise during development phases, because only during the early stages is it possible to alter concepts [8].

For instance in [4], the author aims to understand vibroacoustic early design performance for a FE model by calculating structure-borne noise using energy formulation through input mobility and vibroacoustic transfer functions, and concludes that if main sources of power are connected to the structural frame, any reduction in power input (achieved by altering structure) results in a proportional noise reduction.

Several studies have focused on comparison of different key-performance-indicators (KPIs) with power input, such as in [8] it has been concluded that input power as a key performance indicator turns out to give better correlation to the insertion loss of sound pressure level than that with other KPIs (such as forces or velocities) for changes in design of a simple beam model with elastic connectors. Similar conclusions are obtained for [9], where a simple 2D left rear axle model (assumed to behave linearly and in steady state) is taken as the calculation model and reduced to a network of substructures, for simplified understanding of connections and identification of important power flow paths.

This trend in studies suggest the simplicity of power studies and detailed relation between input power and radiated sound for any mechanical structure. Nonetheless, there is a need to investigate this new direction of research in Volvo Cars that focusses on detailed vehicle body FE models used to scrutinize this relation between power input and radiated noise, and impact of damping modelling within suspension on both as well as their relation.

1.2 Aim and Thesis questions

Aim of this thesis is to investigate the role of damping in basing input power at the forefront of NVH design decisions, and it does so by studying the influence of different modelling of damping within suspension on a number of aspects – firstly, the mechanical input power to trimmed body from suspension due to the excitation, secondly, the interior road noise produced due to this excitation and lastly, the relation between input power and interior noise.

From the foregoing description of research aim and challenges of estimating NVH characteristics, the following thesis question emerges -

How are mechanical power input, cabin noise and their relation dependent on modelling of damping within the suspension?

To be able to answer this question, it is important to understand the complex dynamic relation between input power, cabin noise, and damping within suspension, which leads to the need of following sub-research questions -

1. Which paths contribute majorly to the flow of power from suspension to trimmed body? How does the energy flow vary at different frequencies/frequency ranges?

2. Does a change in MIP produce proportional change in SPL? How can the relation between cabin noise and input power be quantified?

3. How can the quality of correlation between MIP and interior noise be measured?

4. How can impact of damping models, damping values, damping localization, etc. within suspension be captured?

1.3 Objectives

The aim and research questions of this thesis, highlight the need for following research objectives:

- Prepare/choose a suitable calculation model that is simple yet capable to capture most relevant effects for radiation of vibrational power into cabin noise

- Develop a flowchart representing the network of components within vehicle suspension for a simplified yet detailed understanding of connections and power flows from excitation to vehicle body.

- Calculate the power flowing into trimmed body and its contribution from various paths, in order to identify the most crucial paths contributing to the mechanical power input.
- Identify the relation between mechanical input power and cabin noise.
- Identify the dependence of mechanical input power and cabin noise on modelling of damping within a suspension system.

1.4 Structure of Report

A methodology is developed in light of the thesis objectives and divided into different chapters. Firstly, a chapter is dedicated to introducing the vehicle model used for study and discussing its suitability for the research. The next chapter is then focused on developing an understanding of the connections within model by using detailed illustrations and flowcharts of the model. Thirdly, a chapter is dedicated to results. Firstly, results related to calculations of power through various paths into the body, where power flow within system is discussed such that the most important paths and their dominant frequency ranges can be identified to limit the scope of this study. Lastly, a few sections within the chapter of results are dedicated to developing mathematical relation between power and noise as well as studying effects of damping within suspension and body, on the mechanical input power, interior noise and their relation before final conclusions are drawn.

Chapter 2

Theoretical Foundation

This chapter deals with providing definitions of common terminologies used throughout the thesis and necessary theories surrounding them.

2.1 Single-Degree-of-Freedom Systems

A particle or body is said to be vibrating or oscillating if it exhibits a to-and-fro periodic motion about a mean position. Usually, the term oscillation is associated with such motions of low frequency (for e.g. oscillation of a pendulum 1Hz), and the term vibration is associated with high frequency motions (e.g. vibration of a car engine up to a few hundred Hz). So, within vehicle applications, these motions are referred to as automotive vibrations.

Vibration is a complex dynamic phenomenon, that can be extremely complicated to model mathematically and predict the behaviour of vibrating systems, owing to the lack of homogeneity of systems, approximate models, and infinite degrees of freedom a system can possess. Hence, such a system is generally illustrated with ideal springs, masses and dashpots that represent stiffness, inertia and damping within the system. These are the three most important physical quantities that define a dynamic system.

First step in the analysis of a structural vibration problem is making a simplified illustration using inertia, stiffness and damping elements. The simplest form of vibrating system that can be illustrated, is with an ideal spring, an ideal mass and an ideal damper, and is called a Single Degree of Freedom (SDOF/1DOF) system. For example, a generator mounted on its foundation through rubber pads to isolate some or most of its vibrations, can be simplistically modelled as a SDOF system shown in Figure 2.1:

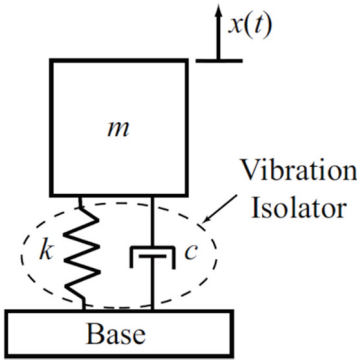

Figure 2.1: SDOF System [1]

Where,

m is the mass of machine,

k is the stiffness of isolator,

c is the damping coefficient of isolator (assuming viscous damping model), and

x is the displacement of mass from mean position.

Table 2.1: SDOF vibration parameters and their units

Quantity	SI-System (MKS)	mm-t-s
Mass (m)	kg	tonne
Stiffness (k)	N.m	N.mm
Damping coefficient (c)	N.s/m	N.s/mm

Table 5.1 shows the commonly used units of dynamic parameters of system which cause three forces to act on this SDOF system, namely the spring force, viscous damping force and external force F, that cause it to accelerate as shown in Figure 2.1. They must be expressed in terms of known constants and variables in order to understand the behaviour of this SDOF system.

As modelled in this system, ideal springs follow Hooke's law, which states that the force acting on a spring (or applied by it) is proportional to its displacement (change in length) and dependent on stiffness k of the spring as given by Equation 2.1.

$$Spring\ force\ =\ kx \tag{2.1}$$

Viscous damping model is widely used to represent vibrational damping within many systems because of its ability to capture roughly the damping effects and also because it makes the system easier to solve. The corresponding viscous damping force is proportional to velocity of damping element and calculated using Equation 2.2.

$$Damping\ force = c\dot{x} \tag{2.2}$$

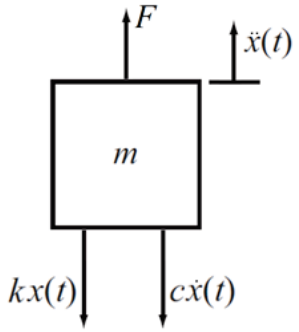

Figure 2.2: Free Body Diagram of SDOF System

Once illustrated as an SDOF system, the next step is formulation of its mathematical model. Applying Newton's Second Law to system is one of the most popular methods of mathematically modelling a SDOF system to obtain its equation of motion.

Making a free body diagram (Figure 2.2) of the SDOF model and applying Newton's Second Law to it gives:

$$\sum \mathbf{F} = m\mathbf{a} \tag{2.3}$$

Where,

$\sum \mathbf{F}$ is the vector sum of forces acting on system, and
$\mathbf{a}$ is the acceleration vector of the system.

$$F - kx - c\dot{x} = m\ddot{x} \tag{2.4}$$

$$m\ddot{x} + c\dot{x} + kx = F \tag{2.5}$$

where, F is the force of excitation/external force applied to the system. Equation 2.5 is a second order, homogeneous, ordinary differential equation in x, known as equation of motion of the SDOF system and provides a relation between forces and kinematic parameters of system. This equation can be solved to obtain dynamic response $x(t)$ of the system.

2.1.1 Complex notations in vibration and Free/Forced vibrations

Equation of motion of a SDOF system is second order differential equation and can be solved either using mathematical integration or alternate methods which convert the ODE to a polynomial equation of degree 2. One such widely used method in engineering dynamics is by representation of sinusoidal force and displacement using complex exponential time functions, as it provides magnitude as well as phase information of system parameters. For example, a sinusoidal excitation force can be expressed as:

$$F = Re(F_0\ e^{i\omega t}) \tag{2.6}$$

Or, according to Euler's formula,

$$F = Re(F_0 cos\omega t + iF_0 sin\omega t) \tag{2.7}$$

Where,

F_0 is the amplitude of applied force, and
ω is the angular frequency of excitation.

Let, $z = z_0\ e^{i(\omega t - \varphi)}$, such that corresponding displacement of mass is expressed as:

$$x = Re(z) \tag{2.8}$$

$$x = Re(z_0\ e^{i(\omega t - \varphi)}) \tag{2.9}$$

Where,

x_0 is the amplitude of applied force
φ is the phase difference between excitation force and displacement

Since, the system is driven by an external excitation frequency, it is highly likely that there would be a phase difference between the applied force and response displacement of the system, and it hence finds its place in Equation 2.9.
Now, substituting complex exponential functions into Equation 2.5 and solving gives:

$$-m\omega^2 z_0\ e^{i(\omega t-\varphi)} + ic\omega z_0\ e^{i(\omega t-\varphi)} + kz_0\ e^{i(\omega t-\varphi)} = F_0\ e^{i\omega t} \tag{2.10}$$

Expressing Equation 2.8 on a complex plane gives Figure 2.3 which is called a phasor diagram, where forces and displacements can be represented as rotating vectors on a complex plane and every time translation is just a rotation. i represents a 90^0 phase shift i^2 a 180^0 phase shift as can be seen from the phasor. It also shows how the applied force (φ radians out of phase with displacement) is a resultant of the spring force (in phase with displacement), damping force (90^0 out of phase with displacement) and inertial force (180^0 out of phase with displacement).

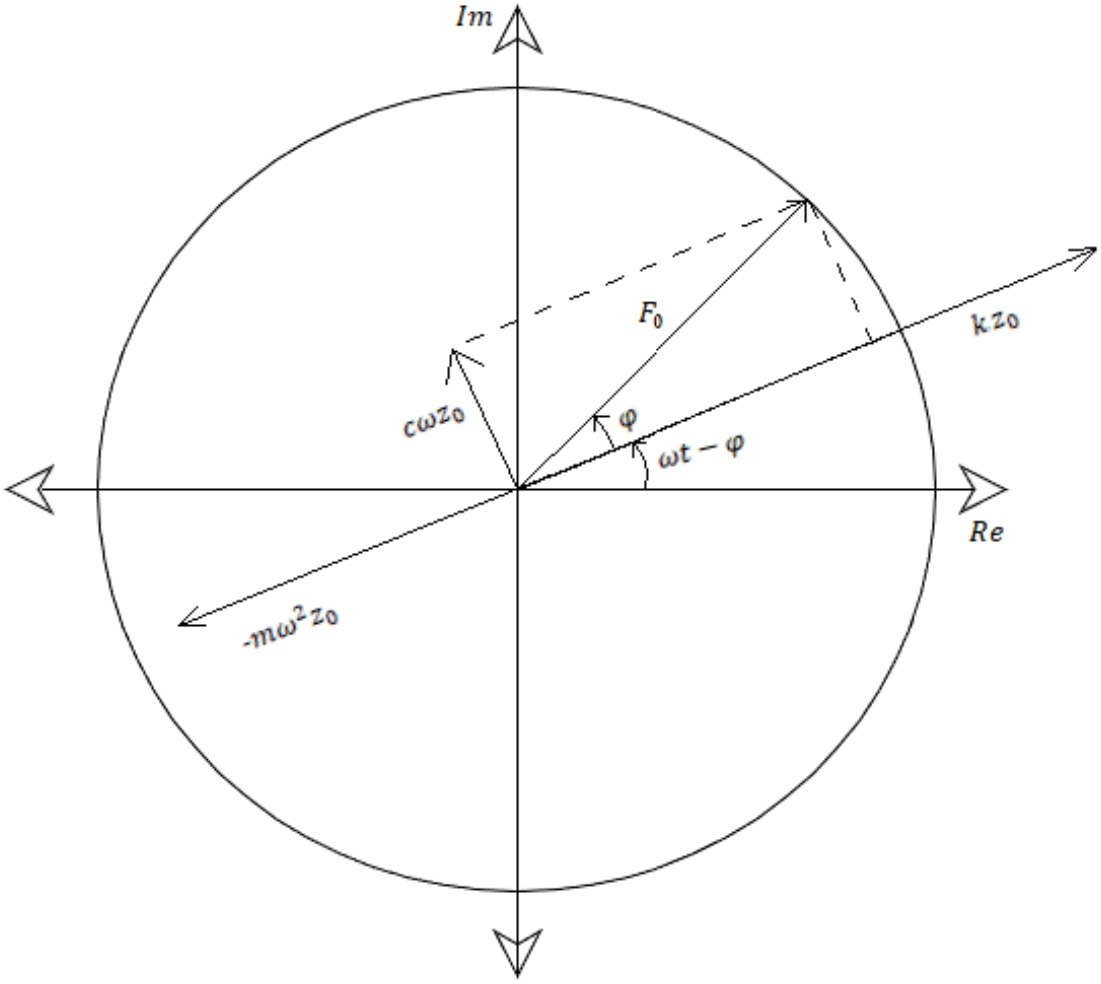

Figure 2.3: Phasor Diagram - SDOF equation on motion expressed in complex plane

The phasor diagram is just a geometrical description of mathematical models and provides great insight into the system behaviour. For example, as seen from phasor diagram, the inertial force relies greatly on the frequency of applied force as it is proportional to ω^2, whereas spring force is independent of vibration frequency and hence

does not contribute significantly to the system behaviour at high frequencies, resulting in a greater phase difference between displacement and applied force. Solving Equation 2.10 further gives a second-degree polynomial in ω as:

$$(-m\omega^2 + ic\omega + k)\ z_0\ e^{-i\varphi} = F_0 \tag{2.11}$$

This equation is much easier to solve than its ODE counterpart and is solved in the next sections.

2.1.2 Free vibrations

For free vibrations, the excitation force is zero and system vibrates freely. The equation of motion for free vibrations of SDOF system is obtained by putting force φ to zero in Equation 2.11 (since there can be no phase difference), such that the following is obtained:

$$(-m\omega^2 + ic\omega + k)\ z_0 = 0 \tag{2.12}$$

Diving the equation be m gives:

$$(-\omega^2 + \frac{ic\omega}{m}\ + \frac{k}{m})\ z_0\ = 0 \tag{2.13}$$

or, the equation can be rewritten as:

$$-\omega^2 + i2\zeta\omega_0\omega\ + \omega_0^2\ = 0 \tag{2.14}$$

Where,

$\omega_0 = \sqrt{\frac{k}{m}}$, is the undamped natural frequency of system
$\zeta = \frac{c}{c_c}$, is the damping ratio of system
$c_c = 2\sqrt{mk}$, is the critical damping of system

Solving for ω in the polynomial Equation 2.14 gives:

$$\omega_{1,2} = \omega_0 \left(i\zeta \pm \sqrt{1-\zeta^2}\right) \tag{2.15}$$

This result of vibration frequency leads to three cases:

1. <u>Underdamped system</u> ($\zeta < 1$):

For underdamped case, Equation 2.15 can be rewritten as,

$$\omega_{1,2} = \omega_0 \left(i\zeta \pm \sqrt{1-\zeta^2}\right) \tag{2.16}$$

Substituting value of $\omega_{1,2}$ into Equation 2.8 gives:

$$z_{1,2} = z_0\ e^{-\zeta\omega_0 t}\ e^{\pm i\sqrt{1-\zeta^2}\omega_0 t} \tag{2.17}$$

So, $x = Re(z)$ gives:

$$x_{1,2} = Re\left(z_0 e^{-\zeta\omega_0 t} e^{\pm i\sqrt{1-\zeta^2}\omega_0 t}\right) \tag{2.18}$$

The basic general solutions are:

$$x_1 = z_0 e^{-\zeta\omega_0 t} cos\left(\omega_0\sqrt{1-\zeta^2}\ t\right) \tag{2.19}$$

$$x_2 = z_0 e^{-\zeta\omega_0 t} sin\left(\omega_0\sqrt{1-\zeta^2}\ t\right) \tag{2.20}$$

The general real solution is calculated by taking linear combination of the two basic solutions. So,

$$x(t) = A_1 e^{-\zeta\omega_0 t} cos\left(\omega_0\sqrt{1-\zeta^2}\ t\right) + A_2 e^{-\zeta\omega_0 t} sin\left(\omega_0\sqrt{1-\zeta^2}\ t\right) \tag{2.21}$$

$$x\,(t) = A_0 e^{-\zeta\omega_0 t} cos\left(\omega_0\sqrt{1-\zeta^2}\ t + \varphi\right) \tag{2.22}$$

It is evident from the expression that:

- The frequency of vibration is $\omega_0\sqrt{1-\zeta^2} = \omega$, called the damped resonant frequency of underdamped SDOF system.
- The $e^{-\zeta\omega_0 t}$ term indicates an exponential decay. So, the amplitude of vibration will exponentially die out because of damping within system.
- φ is the phase angle, indicating the initial condition of position of mass element.

So, the expression can be rewritten as:

$$\boldsymbol{x(t) = A(t)\ cos(\omega t + \varphi)} \tag{2.23}$$

Where, $A(t) = A_0 e^{-\zeta\omega_0 t}$, is the amplitude of vibration

2. Critically damped system $(\zeta = 1)$**:**

For critically damped case, Equation 2.15 can be rewritten as,

$$\omega_{1,2} = i\zeta\omega_0 \tag{2.24}$$

Substituting value of $\omega_{1,2}$ into Equation 2.8 gives:

$$z_{1,2} = z_0\ e^{-\zeta\omega_0 t} \tag{2.25}$$

So, $x = Re(z)$ gives:

$$x_{1,2} = Re(z_0\ e^{-\zeta\omega_0 t}) \tag{2.26}$$

So, the basic general solutions are:

$$x_1 = z_0 e^{-\zeta\omega_0 t} \tag{2.27}$$

$$x_2 = t z_0 e^{-\zeta\omega_0 t} \tag{2.28}$$

The general real solution is calculated by taking linear combination of the two basic solutions. So,

$$\boldsymbol{x\,(t) = (A + Bt)e^{-\zeta\omega_0 t}} \tag{2.29}$$

It is evident from the expression that:

- The equation has no sinusoidal term and hence system does not vibrate.
- The $e^{-\zeta\omega_0 t}$ term indicates an exponential decay of amplitude with time without vibrations.

This case provides the least time in which system can return to its original position.

3. Overdamped system ($\zeta > 1$)**:**

For overdamped case, Equation 2.15 can be rewritten as,

$$\omega_{1,2} = \omega_0 i \left(\zeta \pm \sqrt{\zeta^2 - 1}\right) \tag{2.30}$$

Substituting value of $\omega_{1,2}$ into Equation 2.8 gives:

$$z_{1,2} = z_0 \; e^{(-\zeta \pm \sqrt{\zeta^2-1})\omega_0 t} \tag{2.31}$$

So, $x = Re(z)$ gives:

$$x_{1,2} = Re\left(z_0 \; e^{(-\zeta \pm \sqrt{\zeta^2-1})\omega_0 t}\right) \tag{2.32}$$

So, the basic general solutions are:

$$x_1 = z_0 \; e^{(-\zeta + \sqrt{\zeta^2-1})\omega_0 t} \tag{2.33}$$

$$x_2 = z_0 \; e^{(-\zeta - \sqrt{\zeta^2-1})\omega_0 t} \tag{2.34}$$

The general real solution is calculated by taking linear combination of the two basic solutions. So,

$$\boldsymbol{x(t) = A_1 e^{(-\zeta + \sqrt{\zeta^2-1})\omega_0 t} + A_2 e^{(-\zeta - \sqrt{\zeta^2-1})\omega_0 t}} \tag{2.35}$$

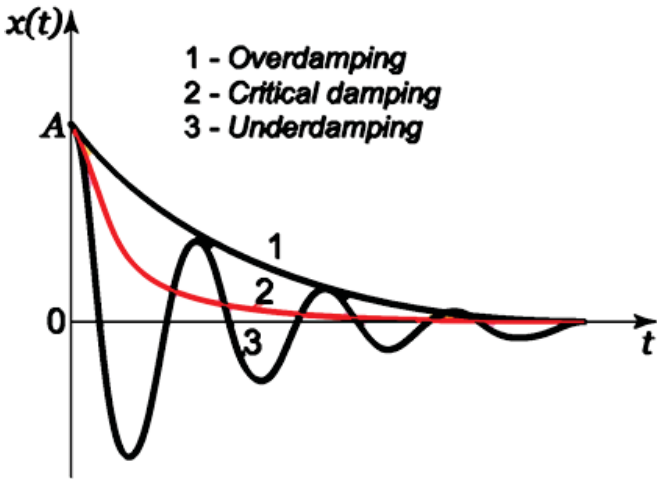

Figure 2.4: Displacement-Time graph of a typical system for all 3 damping cases

It is evident from Equation 2.35 that there is no oscillation, and the two terms decay exponentially. Damping force in the system is so large, that it can control the rate at which mass reaches its original position. Figure 2.4 shows typical case of displacement-time plots for all three damping cases.

2.1.3 Forced vibrations

A system being forced to vibrate under the influence of external excitation is said to be exhibiting forced vibrations. Let, ω_d be the driving frequency of vibrations and δ the phase difference between Force and displacement, then the equation of motion for a SDOF under forced vibrations derived and simplified in previous section is given by Equation 2.11 as:

$$\left(-m{\omega_d}^2 + ic\omega_d + k\right) z_0 e^{-i\delta} = F_0 \tag{2.36}$$

Dividing the equation by m gives:

$$\left(-{\omega_d}^2 + i\frac{c}{m}\omega_d + \frac{k}{m}\right) = \frac{F_0}{mz_0}\left(cos\delta + isin\delta\right) \tag{2.37}$$

Now, rewriting in terms of damping ratio and natural frequency gives:

$$\left(-{\omega_d}^2 + i2\zeta\omega_0\omega_d + {\omega_0}^2\right) = \frac{F_0}{mz_0}\left(cos\delta + isin\delta\right) \tag{2.38}$$

Comparing the real and imaginary terms on both sides of equation gives:

$${\omega_0}^2 - {\omega_d}^2 = \frac{F_0}{mz_0} cos\delta \tag{2.39}$$

$$2\zeta\omega_0\omega_d = \frac{F_0}{mz_0} sin\delta \tag{2.40}$$

Squaring and adding Equations 2.39 and 2.40 gives:

$$z_0 = \frac{F_0/m}{\sqrt{\left({\omega_0}^2 - {\omega_d}^2\right)^2 + 4\zeta^2{\omega_0}^2{\omega_d}^2}} \tag{2.41}$$

Now,dividing equation 2.40 by 2.39 gives:

$$tan\delta = \frac{2\zeta\omega_0\omega_d}{{\omega_0}^2 - {\omega_d}^2} \tag{2.42}$$

Substituting values of z_0 and φ in equation $x = Re\left(z_0 e^{i(\omega_d t - \delta)}\right)$ gives:

$$x = z_0 cos\left(\omega_d t - \delta\right) \tag{2.43}$$

or,

$$x(t) = B\left(\omega_d\right)\ cos\left(\omega_d t - \delta\left(\omega_d\right)\right) \tag{2.44}$$

Here,
$B = z_0$, is the amplitude of vibrations and is a function of ω_d. Also, δ is the phase difference and is a function of ω_d.

Like any other integration problem, the full solution of a second order differential equation must have two free parameters, whereas B and δ are functions of the driving frequency. So, the missing link here is a homogeneous solution of the ODE.

$$\boldsymbol{x(t) = Response\ due\ to\ forced\ input + Free\ Response}$$

Homogeneous solution provides the initial motion of system or free response, that the system was set in before force started acting on it. It dies out as $t \to \infty$. Whereas particular solution provides the steady state solution of this system or response due to forced input. So, the complete solution of forced response of SDOF system is:

$$\boldsymbol{x(t) = Bcos\,(\omega_d t - \delta) + Acos(\omega t + \varphi)} \tag{2.45}$$

So, A and φ are the free parameters which are calculated using initial conditions.

Resonance: As can be seen in Equation 2.41, if the driving frequency equals natural frequency of SDOF system ($\omega_d = \omega_0$), it gives a huge rise in response of the system. This phenomenon is known as resonance and is crucial for understanding dynamic behaviour of systems.

2.2 Multiple-Degree-of-Freedom Systems

Degree of freedom of a system is the number of independent coordinates required to define its configuration. More the degrees of freedom of a system, more are the natural frequencies, and greater the number of ways it can move independently. These types of motion it can exhibit are known as mode shapes and the number of mode shapes = number of natural frequencies = number of DOF.

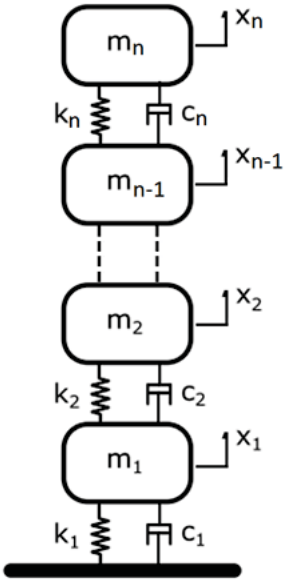

Figure 2.5: n-DOF system

Figure 2.5 shows a MDOF system where n number of masses are present. To fully define the dynamic configuration of this system, coordinates of all n masses are required, hence it is an n-DOF system. Similar to a SDOF system, making a free body diagram of the masses (Figure 2.6) followed by applying Netwon's laws is done to derive equations of motion of this MDOF. Since, there are n-masses in the system, it would have n-equations of motion as below:

$$m_1\ddot{x}_1 + (k_1 + k_2)\, x_1 - k_2 x_2 + (c_1 + c_2)\, \dot{x}_1 - c_2\dot{x}_2 = F_1$$

$$m_2\ddot{x}_2 - k_2 x_1 + (k_2 + k_3)\, x_2 - k_3 x_3 - c_2\dot{x}_1 + (c_2 + c_3)\, \dot{x}_2 - c_3\dot{x}_3 = F_2$$

. . . . . .

. . . . . .

. . . . . .

$$m_{n-1}\ddot{x}_{n-1} - k_{n-1}x_{n-2} + (k_{n-1} + k_n)\, x_{n-1} - k_n x_n - c_{n-1}\dot{x}_{n-2} + (c_{n-1} + c_n)\, \dot{x}_{n-1} - c_n\dot{x}_n = F_{n-1}$$

$$m_n\ddot{x}_n - k_n x_{n-1} + k_n x_n - c_n\dot{x}_{n-1} + c_n\dot{x}_n = F_n$$

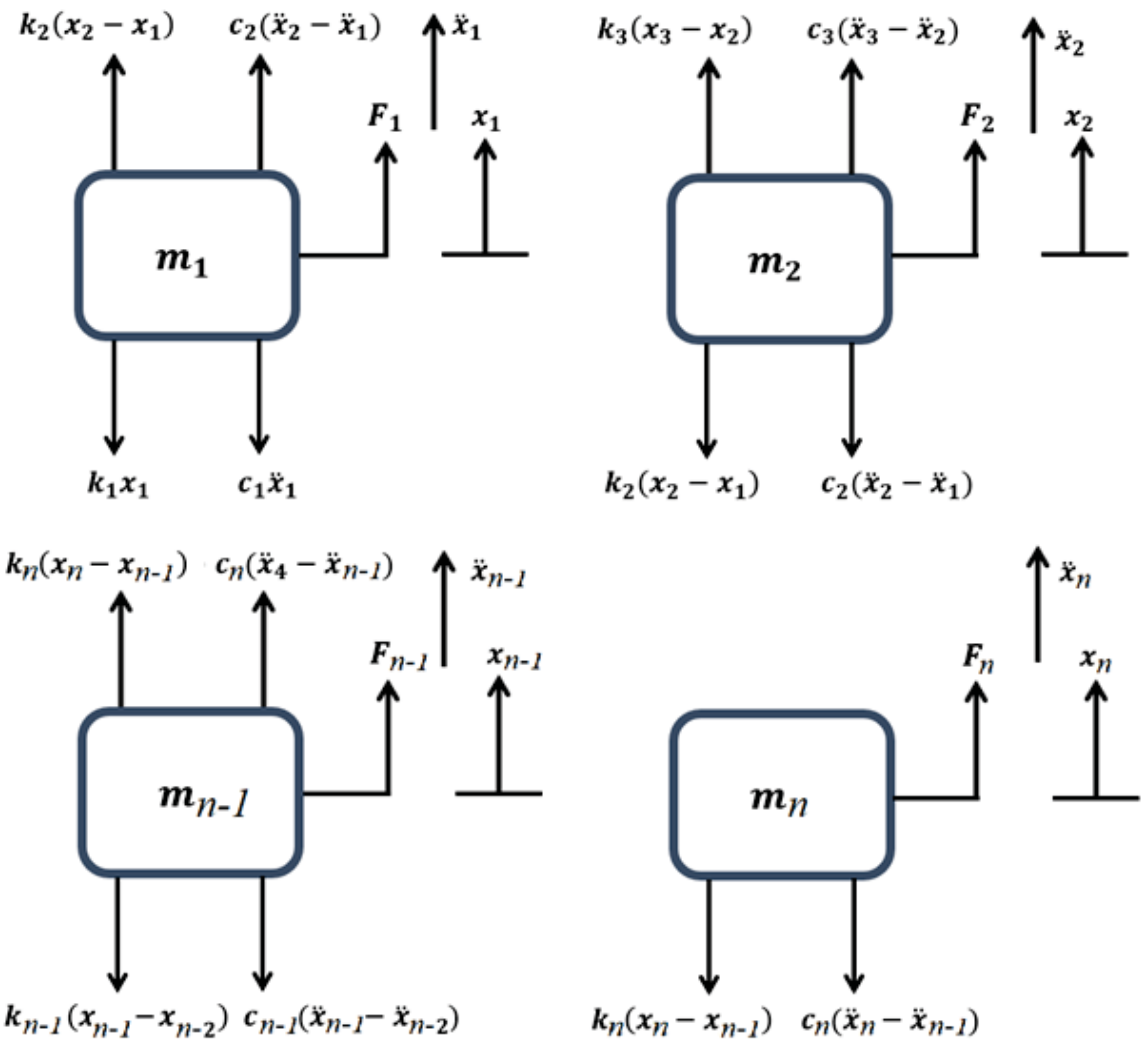

Figure 2.6: FBDs of masses in the MDOF system

It can be seen from the equations that they are interdependent and must be solved simultaneously. Although, there are n equations of motion, they can be dealt in a simplistic and straightforward manner using the tools of matrix algebra. Equation of motion in matrix form can be written as:

$$M\ddot{X} + C\dot{X} + KX = F \tag{2.46}$$

where, each element in the equation is in its matrix form and expressed as given below:

$$M_{N\times N} = \begin{bmatrix} m_1 & 0 & \cdots & 0 & 0 \\ 0 & m_2 & \cdots & 0 & 0 \\ \vdots & \vdots & \ddots & \vdots & \vdots \\ 0 & 0 & \cdots & m_{n-1} & 0 \\ 0 & 0 & \cdots & 0 & m_n \end{bmatrix} \tag{2.47}$$

$$K_{N\times N} = \begin{bmatrix} k_1 + k_2 & -k_2 & \cdots & 0 & 0 \\ -k_2 & k_2 + k_3 & \cdots & 0 & 0 \\ \vdots & \vdots & \ddots & \vdots & \vdots \\ 0 & 0 & \cdots & k_{(n-1)} + k_n & -k_n \\ 0 & 0 & \cdots & -k_n & k_n \end{bmatrix} \tag{2.48}$$

$$C_{N\times N} = \begin{bmatrix} c_1 + c_2 & -c_2 & \cdots & 0 & 0 \\ -c_2 & c_2 + c_3 & \cdots & 0 & 0 \\ \vdots & \vdots & \ddots & \vdots & \vdots \\ 0 & 0 & \cdots & c_{(n-1)} + c_n & -c_n \\ 0 & 0 & \cdots & -c_n & c_n \end{bmatrix} \tag{2.49}$$

$$X_{N\times 1} = \begin{bmatrix} x_1 \\ x_2 \\ \vdots \\ x_{(n-1)} \\ x_n \end{bmatrix} \tag{2.50}$$

$$F_{N\times 1} = \begin{bmatrix} F_1 \\ F_2 \\ \vdots \\ F_{(n-1)} \\ F_n \end{bmatrix} \tag{2.51}$$

2.3 Continuum Formulation

Consider a solid occupying an arbitrary volume V and surface area S as shown in Figure 2.7. dP is a force vector acting on an infinitesimal area dA on surface of the body. Force dP is called a traction vector if dA approaches zero. Mathematically, the traction vector is expressed as:

$$t_i = \begin{bmatrix} t_x \\ t_y \\ t_z \end{bmatrix} = \sigma_{ij} n_i = \begin{bmatrix} \sigma_{xx} n_x + \sigma_{xy} n_y + \sigma_{xz} n_z \\ \sigma_{yx} n_x + \sigma_{yy} n_y + \sigma_{yz} n_z \\ \sigma_{zx} n_x + \sigma_{zy} n_y + \sigma_{zz} n_z \end{bmatrix} \tag{2.52}$$

where, $n_i = \begin{bmatrix} n_x \\ n_y \\ n_z \end{bmatrix}$ is a unit vector acting normal to the surface of body and, σ_{ij} is the stress tensor

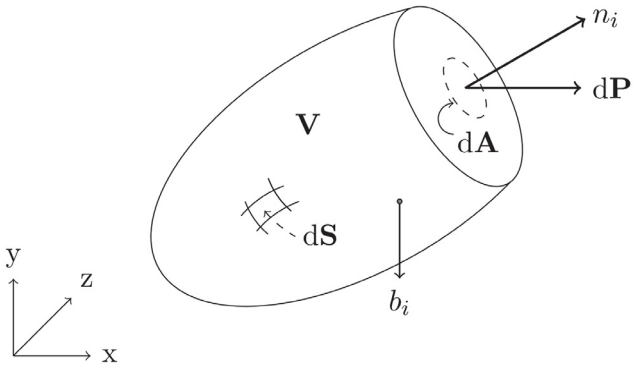

Figure 2.7: Forces on an arbitrary body

For derivation of the strong form of equation of motion, Newton's second law is applied to the arbitrary part of body on which act traction force t_i and body force b_i [6]. This yields:

$$\int_A^S t_i dA + \int_V^S b_i dV = \int_V^S \rho \ddot{u}_i dV \tag{2.53}$$

where, ρ is the density of body, and $\ddot{u}_i$ is the acceleration vector. The formulation here is in terms of the body volume and surface area, which gives way to application of Gauss' divergence theorem for reformulating traction force in terms of volume V as:

$$\int_A^S t_i dA = \int_A^S \sigma_{ij} n_j dA = \int_V^S \sigma_{ij,j} dV \tag{2.54}$$

Where, $\sigma_{ij,j} = \frac{d\sigma_{ij}}{dx_j}$ is the differentiated stress tensor with respect to coordinates x_j. So, Equation 2.53 can be rewritten as,

$$\int_V^S \sigma_{ij,j} dV + \int_V^S b_i dV = \int_V^S \rho \ddot{u}_i dV \tag{2.55}$$

$$\int_V^S (\sigma_{ij,j} + b_i - \rho \ddot{u}_i) dV = 0 \tag{2.56}$$

Simplifying the equation yields:

$$\boldsymbol{\sigma_{ij,j} + b_i = \rho \ddot{u}_i} \tag{2.57}$$

Equation of motion for an arbitrary body is given by Equation 2.57. If the displacement gradients $u_{i,j}$ are considered small, the strain tensor is expressed as:

$$\varepsilon_{ij} = \frac{1}{2}\left(u_{i,j} + u_{j,i}\right) \tag{2.58}$$

Assuming linear-elastic behaviour of the body, the stress-strain relation is expressed as,

$$\sigma_{ij} = D_{ijkl}\varepsilon_{kl} \tag{2.59}$$

where, D_{ijkl} is the elastic stiffness tensor

Boundary conditions are defined as

$$u_i = u_i^{bc} \qquad on\ S^u \tag{2.60}$$

$$t_i = t_i^{bc} \qquad on\ S^u \tag{2.61}$$

known displacement u_i prescribed on S^u and known tractions t_i prescribed on S^t, where S^u and S^t make up the entire surface S.

2.4 Finite Element formulation

This section provides the necessary theoretical background of applying Finite Element Method to solve equation of motion as derived in the previous. First step in FEM is deriving the weak form of Equation 2.57, which can be obtained by multiplying it with an arbitrary weight function v_i that represents virtual displacement, and integrating this product over the volume as given:

$$\int_V^S v_i(\sigma_{ij,j} + b_i - \rho\ddot{u}_i)dV = 0 \tag{2.62}$$

Using Green Gauss theorem and then applying chain rule to the equation gives:

$$\int_V^S v_i\rho\ddot{u}_i dV + \int_V^S v_{i,j}\sigma_{ij}dV = \int_S^S v_i t_i dS + \int_V^S v_i b_i dV = 0 \tag{2.63}$$

The weak form is now developed but a few more steps will be taken to rewrite it. Defining $\varepsilon^v_{ij} = \frac{1}{2}\left(v_{i,j} + v_{j,i}\right)$ and symmetrical σ_{ij} gives:

$$v_{i,j}\sigma_{ij} = \frac{1}{2}\left(v_{i,j}\sigma_{ij} + v_{j,i}\sigma_{ji}\right) = \frac{1}{2}\left(v_{i,j}\sigma_{ij} + v_{i,j}\sigma_{ji}\right) = \varepsilon^v_{ij}\sigma_{ij} \tag{2.64}$$

Second step is to derive the FE formulation by firstly rewriting the quantities in Equation 2.64 in matrix form as given:

$$\varepsilon^v = \begin{bmatrix} \varepsilon^v_{xx} \\ \varepsilon^v_{yy} \\ \varepsilon^v_{zz} \\ 2\varepsilon^v_{xy} \\ 2\varepsilon^v_{yz} \\ 2\varepsilon^v_{zx} \end{bmatrix}; \qquad \sigma_{ij} = \begin{bmatrix} \sigma_{xx} \\ \sigma_{yy} \\ \sigma_{zz} \\ \sigma_{xy} \\ \sigma_{yz} \\ \sigma_{zx} \end{bmatrix}; \qquad \ddot{u} = \begin{bmatrix} \ddot{u}_x \\ \ddot{u}_y \\ \ddot{u}_z \end{bmatrix}; \qquad v = \begin{bmatrix} v_x \\ v_y \\ v_z \end{bmatrix}; \qquad b = \begin{bmatrix} b_x \\ b_y \\ b_z \end{bmatrix}$$

So, the weak from in matrix form can be written as:

$$\int_V^S \rho\boldsymbol{v}^T\ddot{\boldsymbol{u}}dV + \int_V^S (\boldsymbol{\varepsilon^v})^T\boldsymbol{\sigma}dV = \int_S^S \boldsymbol{v}^T\boldsymbol{t}dS + \int_V^S \boldsymbol{v}^T\boldsymbol{b}dV = 0 \tag{2.65}$$

Now, the next step involves approximating displacement vector with global shape function vector $\boldsymbol{N}$ and global displacement vector $\boldsymbol{a}$ as:

$$\boldsymbol{u = Na} \qquad \boldsymbol{=> \ddot{u} = N\ddot{a}} \tag{2.66}$$

Using Galerkin's method to choose weight function v, the following relations can be defined:

$$\boldsymbol{\varepsilon = Ba;} \qquad \boldsymbol{v = Nc;} \qquad \boldsymbol{\varepsilon^v = Bc;} \qquad \boldsymbol{B} = \frac{d\boldsymbol{N}}{dx_i}$$

where, $\boldsymbol{c}$ is an arbitrary weight vector. Using these newly introduced relations, Equation 2.65 can be rewritten as:

$$\boldsymbol{c}^T\left[\left(\int_V^S \rho\boldsymbol{N}^T\boldsymbol{N}dV\right)\ddot{\boldsymbol{a}} + \int_V^S (\boldsymbol{B})^T\boldsymbol{\sigma}dV - \int_S^S \boldsymbol{N}^T\boldsymbol{t}dS - \int_V^S \boldsymbol{N}^T\boldsymbol{b}dV\right] = 0 \tag{2.67}$$

Based on linear elastic material assumption made earlier, following relations can be defined:

$$\boldsymbol{M} = \left(\int_V^S \rho \boldsymbol{N}^T \boldsymbol{N} dV \right) \ddot{\boldsymbol{a}}; \qquad \boldsymbol{K} = (\boldsymbol{B})^T \boldsymbol{\sigma} dV; \qquad \boldsymbol{f} = \int_S^S \boldsymbol{N}^T \boldsymbol{t} dS - \int_V^S \boldsymbol{N}^T \boldsymbol{b} dV$$

where, $\boldsymbol{M}$, $\boldsymbol{K}$ are the mass and stiffness matrix and $\boldsymbol{f}$ is the force vector. Since, c is arbitrary, Equation 2.67 can be rewritten as:

$$\boldsymbol{M}\ddot{\boldsymbol{a}} + \boldsymbol{K}\boldsymbol{a} = \boldsymbol{f} \tag{2.68}$$

his equation of motion represents a system without damping. For example, viscous damping can be introduced in the system by adding a term $\boldsymbol{C}\dot{\boldsymbol{a}}$, where $\boldsymbol{C}$ is the damping matrix.

$$\boldsymbol{M}\ddot{\boldsymbol{a}} + \boldsymbol{C}\dot{\boldsymbol{a}} + \boldsymbol{K}\boldsymbol{a} = \boldsymbol{f} \tag{2.69}$$

Equation 2.67 provides the FE form of equation of motion for an arbitrary body occupying volume V.

2.5 Structural Dynamic Analysis

This section deals with the various ways of analyzing a MDOF dynamic system (and the steps involved in it), such as the one represented by Equation 2.69.

2.5.1 Free undamped vibration

The equation of motion for an undamped MDOF system with no forces acting on it, can be represented as:

$$\boldsymbol{M\ddot{a}} + \boldsymbol{Ka} = 0 \tag{2.70}$$

Assuming response of the system to be harmonic, given by:

$$a(t) = \hat{A}e^{i\omega t}\phi \tag{2.71}$$

where, $\hat{A}$ is the complex amplitude,
and, ϕ is a time independent constant vector Differentiating Equation 2.71 with respect to time and substituting the result into equation 35 yields,

$$\left(K - \omega^2 M\right)\phi = 0 \tag{2.72}$$

For a non-trivial solution to the eigenvalue problem,

$$det\left(K - \omega^2 M\right) = 0 \tag{2.73}$$

If the MDOF system has n-DOFs, there would be n solutions or eigenfrequencies $\omega_j = \omega_1, \omega_2 \ldots \omega_n$. Corresponding to each eigenfrequency will be a mode shape or eigenmode (vibrational pattern), which is obtained by substituting calculated eigenfrequency into Equation 2.72. Then, solution to Equation 2.71 can be represented as a sum of eigenmodes because of its orthogonality as:

$$\boldsymbol{a}\left(t\right) = \sum_{j=1}^{n} q_j\left(t\right)\phi_j \tag{2.74}$$

where, $q_j\left(t\right) = \hat{q}_j\left(t\right)e^{i\omega t}$, and the complex amplitude $\hat{q}_j$ of ϕ_j is determined by initial conditions.

2.5.2 Forced undamped harmonic vibration

The equation of motion for an undamped MDOF system experiencing a harmonic excitation is represented by:

$$\boldsymbol{M\ddot{a}} + \boldsymbol{Ka} = \hat{\boldsymbol{f}}e^{i\omega t} \tag{2.75}$$

where, $\hat{f}$ is the complex amplitude of force

As discussed in previous SDOF section, full solution of Equation 2.75 contains a homogeneous solution (obtained in Equation 2.74, by solving the free response) and a particular solution which is the steady state response and hence independent of

initial conditions. The particular solution can be derived by assuming a harmonic solution as:

$$a(t) = \hat{a}e^{i\omega t} \tag{2.76}$$

and, $\hat{a}$ is a time independent constant vector. Differentiating Equation 2.76 with respect to time and substituting the result into Equation 2.75 yields,

$$\left(K - \omega^2 M\right)\hat{a} = \hat{f} \tag{2.77}$$

Multiplying 2.77 with eigenmodes $\boldsymbol{\phi}_k^{\boldsymbol{T},(k=1,2,...,k)}$, and modally decomposing $\hat{a}$ as,

$$\hat{\boldsymbol{a}} = \sum_{j=1}^{n} \hat{r}_j(t)\boldsymbol{\phi}_j \tag{2.78}$$

the following equation is obtained:

$$-\omega^2 \sum_{j=1}^{n} \boldsymbol{\phi}_k^T \boldsymbol{M}\boldsymbol{\phi}_j \hat{r}_j + \sum_{j=1}^{n} \boldsymbol{\phi}_k^T \boldsymbol{K}\boldsymbol{\phi}_j \hat{r}_j = \boldsymbol{\phi}_k^{\boldsymbol{T}}\hat{\boldsymbol{f}} \tag{2.79}$$

Considering orthogonal eigenmodes, $\boldsymbol{\phi}_k^{\boldsymbol{T}}\boldsymbol{M}\boldsymbol{\phi}_j$ and $\boldsymbol{\phi}_k^{\boldsymbol{T}}\boldsymbol{K}\boldsymbol{\phi}_j\hat{r}_j$ are zero for if $j \neq k$. This yields n independent systems represented by:

$$-\omega^2 \bar{m}_j \hat{r}_j + \bar{k}_j \hat{r}_j = \bar{f}_j \tag{2.80}$$

Where, $\bar{m}_j = \boldsymbol{\phi}_k^{\boldsymbol{T}}\boldsymbol{M}\boldsymbol{\phi}_j$, $\bar{k}_j = \boldsymbol{\phi}_k^{\boldsymbol{T}}\boldsymbol{K}\boldsymbol{\phi}_j\hat{r}_j$ and $\bar{f}_j = \boldsymbol{\phi}_k^{\boldsymbol{T}}\hat{\boldsymbol{f}}$ $(j = 1, 2..., n)$ The amplitude corresponding to each eigenmode is obtained from the each of the n uncoupled systems as:

$$\hat{r}_j = \frac{\bar{f}_j}{\bar{k}_j} \frac{1}{1 - (\omega/\omega_j)^2} \tag{2.81}$$

Where, $\omega_j = \sqrt{\frac{\bar{k}_j}{\bar{m}_j}}$
Hence, the steady state solution and homogeneous solution of Equation 2.75 can be obtained using equations derived above as:

$$\boldsymbol{a}(t) = e^{i\omega t} \sum_{j=1}^{n} \frac{\bar{f}_j}{\bar{k}_j} \frac{1}{1 - (\omega/\omega_j)^2} \phi_j + \sum_{j=1}^{n} q_j(t)\phi_j \tag{2.82}$$

2.5.3 Forced harmonic vibration on a damped system

The equation of motion for a viscous damped MDOF system experiencing a harmonic excitation is represented by:

$$\boldsymbol{M}\ddot{\boldsymbol{a}}(t) + \boldsymbol{C}\dot{\boldsymbol{a}}(t) + \boldsymbol{K}\boldsymbol{a}(t) = \boldsymbol{f}(t) \tag{2.83}$$

Using the concepts of modal contribution to assume same steady state solution as in equation 41 and similar modal expansion as in Equation 2.78 yields:

$$-\omega^2 \sum_{j=1}^{n} \boldsymbol{\phi}_k^T \boldsymbol{M}\boldsymbol{\phi}_j \hat{r}_j + i\omega \sum_{j=1}^{n} \boldsymbol{\phi}_k^T \boldsymbol{C}\boldsymbol{\phi}_j \hat{r}_j + \sum_{j=1}^{n} \boldsymbol{\phi}_k^T \boldsymbol{K}\boldsymbol{\phi}_j \hat{r}_j = \boldsymbol{\phi}_k^{\boldsymbol{T}}\hat{\boldsymbol{f}} \tag{2.84}$$

Considering orthogonal eigenmodes, $\boldsymbol{\phi}_k^{\boldsymbol{T}}\boldsymbol{M}\boldsymbol{\phi}_j, \boldsymbol{\phi}_k^{\boldsymbol{T}}\boldsymbol{C}\boldsymbol{\phi}_j\hat{r}_j$ and $\boldsymbol{\phi}_k^{\boldsymbol{T}}\boldsymbol{K}\boldsymbol{\phi}_j\hat{r}_j$ are zero for if $j \neq k$. This yields n independent systems represented by:

$$-\omega^2\bar{m}_j\hat{r}_j + i\omega\bar{c}_j\hat{r}_j + \bar{k}_j\hat{r}_j = \bar{f}_j \tag{2.85}$$

Where, $\bar{m}_j = \boldsymbol{\phi}_k^{\boldsymbol{T}}\boldsymbol{M}\boldsymbol{\phi}_j$, $\bar{c}_j = \boldsymbol{\phi}_k^{\boldsymbol{T}}\boldsymbol{C}\boldsymbol{\phi}_j\hat{r}_j$, $\bar{k}_j = \boldsymbol{\phi}_k^{\boldsymbol{T}}\boldsymbol{K}\boldsymbol{\phi}_j\hat{r}_j$ and $\bar{f}_j = \boldsymbol{\phi}_k^{\boldsymbol{T}}\hat{\boldsymbol{f}}(j = 1, 2..., n)$

Introducing the damping ratio term represented by:

$$\zeta_j = \frac{\bar{c}_j}{2\bar{m}_j\omega_j} \tag{2.86}$$

Rewriting Equation 2.86 in terms of the damping ratio gives:

$$-\omega^2\bar{m}_j\hat{r}_j + 2i\omega\zeta_j\omega_j\hat{r}_j + \bar{k}_j\hat{r}_j = \bar{f}_j \tag{2.87}$$

The amplitude corresponding to each eigenmode is obtained from the each of the n uncoupled systems as:

$$\hat{r}_j = \frac{\bar{f}_j}{{\omega_j}^2}\frac{1}{1 - (\omega/\omega_j)^2 + 2i\zeta_j(\omega/\omega_j)} \tag{2.88}$$

Since, the system is damped, its transient response would die out very soon. Hence, the steady state solution can be treated as the complete solution of Equation 2.83 given by:

$$\boldsymbol{a}(t) = e^{i\omega t}\sum_{j=1}^{n}\frac{\bar{f}_j}{{\omega_j}^2}\frac{1}{1 - (\omega/\omega_j)^2 + 2i\zeta_j(\omega/\omega_j)}\boldsymbol{\phi}_j \tag{2.89}$$

2.5.4 Frequency Response Function

Frequency Response Function (FRF) is a dynamic response analysis tool used in the frequency domain to understand how a structure transmits vibration. FRF of a point within a linear, time-invariant system is a measure of the steady state response of the point due to a unit harmonic load acting at the same point or another. FRF contains the amplitude as well as phase information for the system parameter. For a damped system under harmonic load represented by Equation 2.83, FRF is represented by:

$$H(\omega) = \frac{\hat{a}}{\hat{f}} = \frac{1}{K + i\omega C - \omega^2 M} \tag{2.90}$$

In modal coordinates, obtained by modal decomposition of the given system, FRF is represented as:

$$H_j = \frac{1}{{\omega_j}^2}\frac{1}{1 - (\omega/\omega_j)^2 + 2i\zeta_j(\omega/\omega_j)} \tag{2.91}$$

The FRF stated in equation above is known as Dynamic Stiffness. Simply stated, FRF is a transfer function or output divided by input, and depending on which

parameter is considered the output, FRF can be of many different types. For example, in case of mechanical systems where force is the input, there are three common FRFs, namely Dynamic Stiffness (Displacement/Force), Mobility (Velocity/Force) and Accelerance (Acceleration/Force).

$$(Mobility)\ M_j = \frac{1}{{\omega_j}^2} \frac{i\omega}{1 - (\omega/\omega_j)^2 + 2i\zeta_j\,(\omega/\omega_j)} \tag{2.92}$$

$$(Accelerance)\ A_j = \frac{1}{{\omega_j}^2} \frac{-\omega^2}{1 - (\omega/\omega_j)^2 + 2i\zeta_j\,(\omega/\omega_j)} \tag{2.93}$$

Each FRF has its own advantages and is used to extract a different dynamic parameter of the system, but most common observations from FRFs are firstly, natural frequencies of a system (peaks in spectrum indicate resonances), secondly, damping (proportional to width of peaks), thirdly, mode shapes (using amplitude and phase data), and many more. FRFs are also calculated experimentally by firstly converting discrete time signals into frequency domain by fast fourier transformation (FFT) of them.

2.6 Damping Models

Damping within a system is its ability to dissipate mechanical energy, usually by converting it into heat. There can be a large number of factors that lead to damping within a system such as internal friction, mechanical hysteresis, joint friction, microscopic/macroscopic defects, opening and closure of microcracks, acoustic radiation, structural radiation, etc. Such factors make damping a highly complex phenomena and almost impossible to rely entirely on mathematical models for realistically capturing the effects of damping within a system. Instead, to predict the dynamic behaviour of system with higher accuracy, modal damping ratios are considered which are obtained empirically using actual response data, having less assumptions and able to accommodate more non-linear behaviour of damping within structures.

Like every other engineering mechanics problem, mathematical model is a great starting point and there are a few damping models that are commonly used for modelling damping within different systems depending on their suitability like Viscous Damping, Structural Damping, Proportional Damping, Coulomb Damping, etc. The scope of this thesis is limited to viscous and structural damping models that are described further in this section.

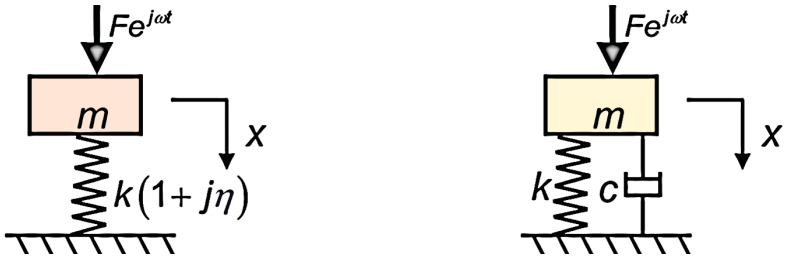

Figure 2.8: (a) Structural and (b) Viscous Damping in SDOF

2.6.1 Viscous damping model

Viscous damping model is usually represented by a dashpot as shown in Figure 2.8 as it is a good representation of damping within automotive damped and such damping mechanisms. Equation of motion for an SDOF system with viscous damping experiencing forced harmonic vibrations is given by:

$$m\ddot{x}(t) + c\dot{x}(t) + kx(t) = f(t) \tag{2.94}$$

Where, damping force $F_d = c\dot{x}$, and is proportional to the velocity. So, the energy dissipated per cycle can be calculated as:

$$W_d = \int F_d dx \tag{2.95}$$

expressing damping force in terms of damping coefficient and velocity gives:

$$W_d = \int c\dot{x} dx \tag{2.96}$$

But, $dx = \dot{x}dt$. So,

$$W_d = \int_0^{\frac{2\pi}{\omega}} c\dot{x}^2 dt \tag{2.97}$$

For a harmonic output, let the response would for this SDOF be

$$x = Xcos\,(\omega t - \phi) \tag{2.98}$$

Differentiating with respect to time gives:

$$\dot{x} = -\omega X sin\,(\omega t - \phi) \tag{2.99}$$

Putting the value of $\dot{x}$ in Equation 2.97 gives:

$$W_d = \int_0^{\frac{2\pi}{\omega}} c\,[-\omega X sin\,(\omega t - \phi)]^2 dt \tag{2.100}$$

Solving the integral yields:

$$W_d = \pi c \omega X^2 \tag{2.101}$$

rewriting in terms of damping ratio and frequency gives:

$$W_d = \pi m 2\zeta \omega^2 X^2 \tag{2.102}$$

Note:

1. Viscous damping force is proportional to and in-phase with velocity
2. The energy dissipated per cycle is proportional to the frequency of vibration, square of amplitude of vibrations

2.6.2 Structural damping model

Structural (or Hysteretic) damping model is usually represented by a complex stiffness as shown in Figure 2.8. It is a good representation of damping within viscoelastic materials for their non-linear behaviour caused due to the hysteresis losses. Some material properties like elasticity(E), stiffness(k) are defined as:

$$\bar{E} = E_{Re} + iE_{Im} \tag{2.103}$$

$$\bar{k} = k_{Re} + ik_{Im} \tag{2.104}$$

Where, E_{Re} is called the storage modulus and E_{Im} loss modulus

Now, a new parameter called loss factor (η) is introduced, given by:

$$\eta = \frac{E_{Re}}{E_{Im}} = \frac{k_{Re}}{k_{Im}} = tan\delta \tag{2.105}$$

Where, δ is called the loss angle.
Equation of motion for an SDOF system with structural damping experiencing forced harmonic vibrations is given by:

$$m\ddot{x}(t) + k(1 + i\eta)x(t) = f(t) \tag{2.106}$$

The loss factor is also defined as:

$$\eta = \frac{Energy\ dissipated\ in\ a\ cycle}{Total\ energy} \tag{2.107}$$

Let, c_{eq} be the equivalent viscous coefficient. Then loss factor is:

$$\eta = \frac{\pi c_{eq} \omega X^2}{2\pi \left(\frac{1}{2} k X^2\right)} \tag{2.108}$$

on solving,

$$\eta = \frac{c_{eq}\omega}{k} \tag{2.109}$$

Note:

1. Structural damping force is proportional to displacement and in-phase with velocity
2. Structural damping depends on material type, and the constant stiffness and loss factor are valid only for harmonic force
3. Structural damping work is independent of velocity and frequency

At resonance ($\omega = \omega_n$), consider a viscous damping system with damping factor ζ and damping coefficient c_{eq}, that has the same equivalent dissipation over a cycle as the structural damping model. Then the loss factor can be rewritten as:

$$\eta = \frac{2m\zeta {\omega_n}^2}{k} \tag{2.110}$$

or,

$$\eta = \frac{2\zeta {\omega_n}^2}{\frac{k}{m}} \tag{2.111}$$

Since, $\omega_n = \sqrt{\frac{k}{m}}$, the equation can be rewritten as:

$$\boldsymbol{\eta = 2\zeta} \tag{2.112}$$

So, at resonance, for equivalent dissipation by structural and viscous damping models, they must follow the relation in Equation 2.112.

2.7 Road Noise

A vehicle cabin is subjected to three major sources of noise and vibration, namely engine and power-train excitation (due to direct connection with the body), wind excitation (due to air friction acting on body) and road excitation (due to contact between road and tires). So, a refined vehicle from NVH perspective, needs to have low response due to these excitation.

Noise produced due to contact between moving tires and road, transmitted through structure-borne as well as air-borne paths to the interior of vehicle is known as road noise. The term road noise might seem misleading, as it does not involve noise produced in the exterior of vehicle due to the contact between tires and road, which is commonly known as tire noise. Vehicle interior road noise is of frequencies below 1000 Hz (low-frequency range), and can be classified into:

- Structure-borne road noise:
  - Transferred through vehicle suspension from tire
  - Predominant at frequencies < 400 Hz
- Airborne road noise:
  - Transferred through vehicle structure from tire
  - Predominant at frequencies > 400 Hz

These two are entirely different physical phenomena and usually dealt with separately. This thesis deals with only the structure-borne road noise and it will commonly be referred to as road noise throughout the text hereon.

For Road noise analysis, the first step is identification of excitation points, response points and the transfer paths, second is freezing the response and excitation quantities such as force at body interface points, noise at driver's ear, etc. Lastly, measurement of these excitation and response parameters needs to be done for further analysis. For example, staying within the scope of this thesis of studying road noise, firstly, excitation point is considered as tire patch and the response points as the microphone locations at driver and passengers' ears. Secondly, the input parameter is considered as the force acting on tire patch due to its interaction with road and output parameter the noise signal obtained at microphone locations. Lastly, these forces are usually measured using accelerometers at the excitation points while driving vehicle on a track or by applying similar load to CAE model of car at the excitation points, depending on the scope of study. For cabin noise, sound pressure level (SPL) values at the microphone locations are obtained experimentally or through NVH CAE analysis. The SPL values at individual microphone or averaged sum as given by Equation 2.113, can be expressed on a decibel (dB) scale, or on pressure scale depending on analysis required.

$$SPL_{mean}(f) = \frac{1}{n}\sum_{i=1}^{n} SPL_i(f) \tag{2.113}$$

where,

SPL_{mean} is the averaged SPL,
SPL_i is the sound pressure measure at i^{th} location,
n is the number of response points (= 4, generally), and
f denotes the frequency domain in which SPL is measured.

To express SPL in dB scale, the following equation is used:

$$SPL_{dB} = 20log_{10}\left(\frac{SPL_{mean}\,(f)}{P_0}\right) \tag{2.114}$$

where,
SPL_{dB} is the averaged SPL in decibel scale,
and, $P_0 = 2 \times 10^{-5}\ Pa$ is the reference pressure.

Additionally, it is crucial to have a good understanding of the transfer paths for road noise analysis, as some dominant structural parts cause most of the peaks in frequency spectrum of road noise. For example, low frequency peaks in structure-borne road noise spectra are commonly attributable to:

- Acoustic modes of cabin space
- Vibrational modes of tire structure
- Acoustic modes of tire cavity

2.8 Mechanical Input Power

In this dissertation, the cycle mean power input is referred to as Mechanical Input Power, and for a continuous system can be derived using the linear elastic wave equation given by:

$$\frac{\partial E_{totV}}{\partial t} + \boldsymbol{\nabla I} = -D \tag{2.115}$$

Where,

E_{totV} is the total energy density of system contained in control volume V and
$\boldsymbol{I}$ is the instantaneous mechanical intensity or vector of acoustic energy fluence.

Also, $\boldsymbol{I} = \sigma v$. Where,

σ is the stress tensor and v the velocity vector.
D is the rate of dissipated energy per volume or dissipation power density.

Integrating Equation 2.115 over the control volume V and using divergence theorem gives:

$$\frac{\partial}{\partial t}\int_V E_{totV} dV + \int_S \boldsymbol{I}.\boldsymbol{n} dS = -\int_V D dV \tag{2.116}$$

Let, $P = \int_S \boldsymbol{I}.\boldsymbol{n} dS$ and $P_{diss} = -\int_V D dV$, such that P is the instantaneous power out of surface S and is calculated by the surface integral of scalar product of the mechanical intensity and surface normal vector ($\boldsymbol{n}$) and P_{diss} is the dissipated power. Then,

$$P = \int_S \boldsymbol{I^T}.\boldsymbol{n} dS = \int_S \boldsymbol{n}^T \boldsymbol{\sigma v} dS \tag{2.117}$$

In steady state harmonic conditions, mean power can be calculated as:

$$\bar{P} = \frac{1}{T}\int_0^T P dt = \frac{1}{T}\int_0^T P_{diss} dt \tag{2.118}$$

Where, T is the time period of harmonic cycle. Steady state systems are usually dealt in frequency domain and following the relation of complex quantities $\hat{a}$ and $\hat{b}$ in complex domain as $\Re(\hat{a}).\Re(\hat{b}) = \frac{1}{2}\Re(\hat{a}.\hat{b}^*)$, where $*$ denotes conjugate complex. Complex power can be expressed as:

$$\hat{P} = \frac{1}{2}\int_S \boldsymbol{n}^T \hat{\boldsymbol{\sigma}} \hat{\boldsymbol{v}}^* dS \tag{2.119}$$

Now, for steady state conditions, the cycle average of total energy is constant $\left(or, \quad \frac{\partial}{\partial t}\int_V^O E_{totV} dV = 0\right)$ so the Equation 2.115 can be rewritten as:

$$0 + \hat{P}_{out} = -\hat{P}_{diss} \tag{2.120}$$

or, for power into the system -

$$-\hat{P}_{in} = -\hat{P}_{diss} \tag{2.121}$$

$$\hat{P}_{in} = \hat{P}_{diss} \tag{2.122}$$

So, in steady state conditions, the cycle average power into a system equals the cycle-average of the dissipated power of system. The cycle averaged power $\bar{P}$ also known as active power corresponds to the real part of complex power $\hat{P}$, and is the power that is dissipated due to damping present within system. Imaginary part of complex power is the reactive power whose time averaged value is zero and is hence not relevant to the study [5].

$$\bar{P} = \mathfrak{R}(\hat{P}_{diss}) = \mathfrak{R}(\hat{P}_{in}) \tag{2.123}$$

Equation 2.119 provides a means to calculate power for continuous systems, but calculation is simplified further for a finite element model by defining it as the sum of time averaged product of nodal forces (and moments) with the in-phase component of corresponding nodal velocities (and angular velocities), for all nodes that are an input loading point for the component [3], [5]. For time harmonic analysis, where complex quantities are used, this operation is the same as multiplying force (and moment) vector by the Hermitian transpose of velocity (and angular velocity) vector, or vice versa.

Active mean power is expressed in terms of nodal dynamic parameters as:

$$\bar{P} = \frac{1}{2}\mathfrak{R}\ (\hat{f}^*.\hat{v} + \hat{M}^*.\hat{\omega}) \tag{2.124}$$

Where,

$\hat{f}$ is the nodal force vector
$\hat{v}$ is the nodal velocity vector
$\hat{M}$ is the nodal moment vector
$\hat{\omega}$ is the nodal angular velocity vector

Using the equation for active power, mechanical power input to any component can be calculated in FE models if the values for required nodal dynamic parameters are available for input nodes. Since, power is a scalar quantity, a positive power exchange means power input to the component, and a negative power exchange means power being lost to the source. The term active power refers to mechanical input power in this thesis unless mentioned otherwise.

Chapter 3

Example Vehicle Model

This section deals with either developing a new model or choosing a pre-existing vehicle model that is able to provide necessary output values using which can be calculated power and interior road noise values. Road noise calculation involves three subsystems within the vehicle, namely wheels, suspension and body. So, the calculation model to be developed for this dissertation must contain at least a trimmed body and a suspension system, simple enough to be studied within the available time frame and yet detailed enough to:

- Represent all major parts of a car available to the road noise team in early development phases
- Provide nodal forces and displacements/velocities of various interface points within the model for an applied load case
- Allow for change of damping parameters within the suspension components (such as link arm, subframe, etc.) as well as connectors (bushings, ball joints, etc.) within the model
- Capture all relevant effects of varying damping parameters on suspension and trimmed body components
- Capture sound pressure produced at mic locations near occupants' ears within the trimmed body cabin

The simulation model chosen is a concept BEV (Battery Electric Vehicle) wheel suspension model with Continental tires (not shown due to confidentiality), to which is attached a suitable trimmed body (example of trimmed body shown in Figure 3.1) that includes air as the fluid medium within the cabin cavity and four mic locations to capture noise produced at occupants' outer ears (1 driver and 3 passengers).

Damping within the suspension in calculation model is generalized at 8% structural damping into all the components and 5% structural damping into all the bushes (not the RBE2 elements for rigid connectors).

The rear left and rear right tires given in the calculation model consist of 177 tag points each that collectively behave as tire patch to be used as source for model excitation.

For this study, a simplified load case is devised with excitation in the form of displacement instead of force. Only the left tire patch is excited with vertical displacement of 0.01 mm in an entire frequency range from 10 – 400 Hz, while vehicle model is simulated to be travelling at 80kmph.

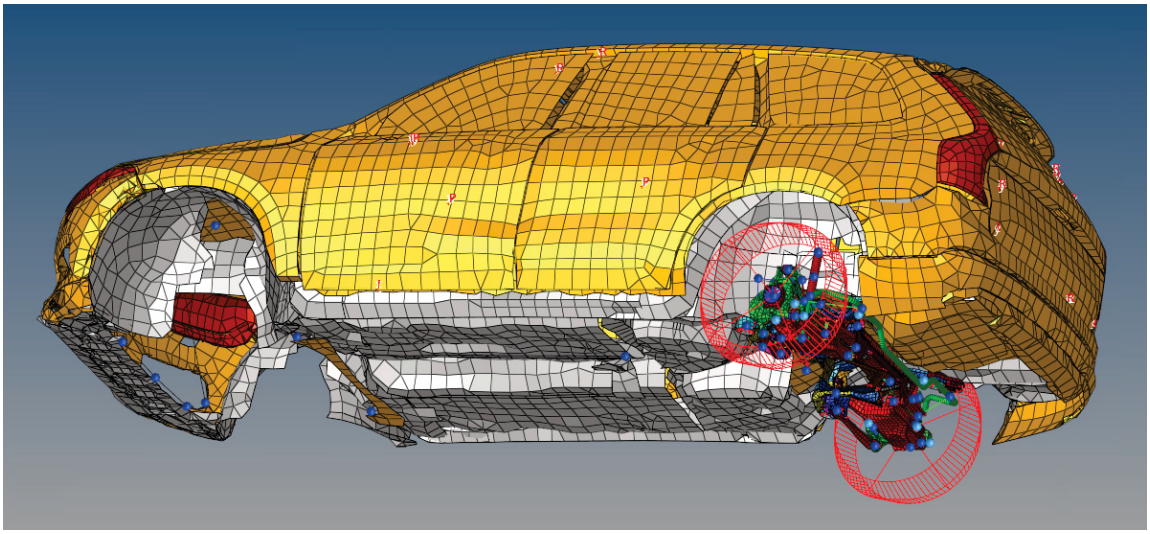

Figure 3.1: Trimmed body and rear suspension model of Volvo XC90

The model so chosen can be useful for the team at Volvo Cars to benefit from thesis outcomes in the long run. It is detailed enough to be able to capture all relevant quantities such as MIP, SPL as well as vary damping in different parts of the model. The results can be extrapolated for other load cases and more detailed models. Since, the road noise team works on Altair Optistruct and NVH Director for their NVH simulations, which are dynamics tools able to capture all the details required for the study in frequency domain, the simulation model is chosen in accordance with the team's expertise as well.

Chapter 4

Network Representation

The calculation model consists of more than a hundred parts joined together to transmit power from tire to the trimmed body. These connections are usually very complex, and at first glance almost impossible to estimate the details of how power flows from source all the way into trimmed body.

To deal with this complexity, a flowchart is prepared in this chapter that diagrammatically represents all components within the model as well as the connections between them in detail. Figure 4.1 shows an example of a rear suspension model, suspension components, body interface points, and some connections that need to be represented in the flowchart.

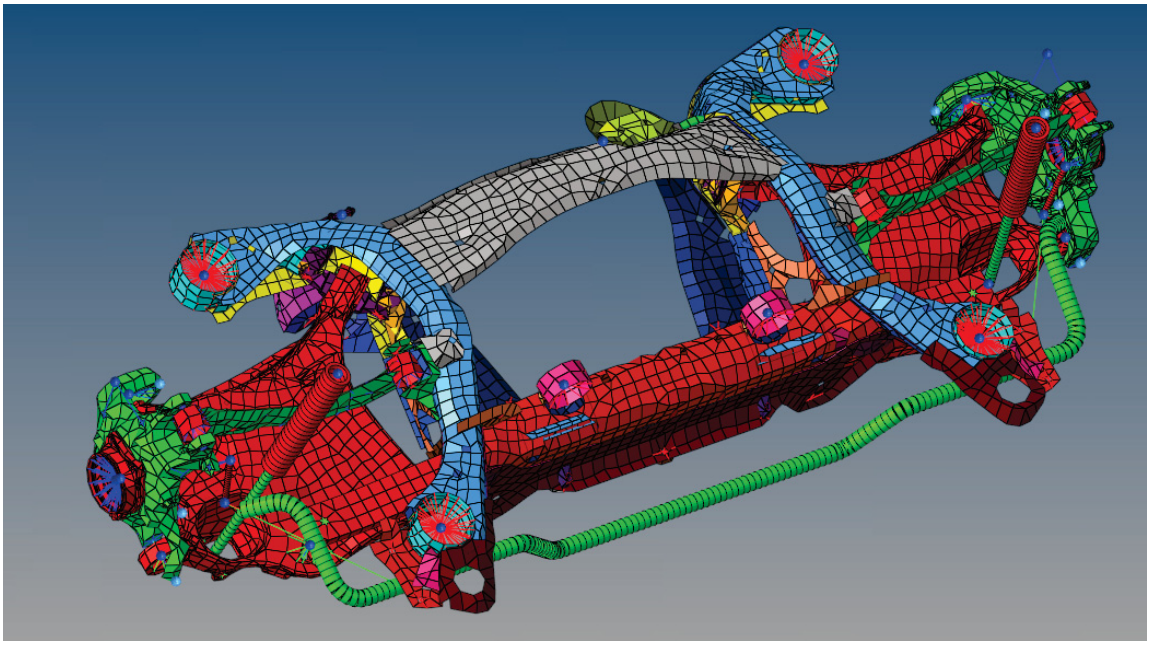

Figure 4.1: Model of an XC90 rear suspension

To deal with the requirement of developing a network representation, a plan is devised as follows. Components are represented by a box, with their respective names written inside as shown in Figure 4.2. Arrows are used to depict a connection between components, where the arrow heads point in positive direction of power flow. To understand how any two components are connected, the IDs of their linked nodes are given below the arrow connecting them, and the ID (in software) of connector mentioned on top of the arrow. For example, starting from the left hub as source

of excitation, its connection to neighbouring components is represented by arrows (pointing towards trimmed body, to represent positive direction of power flow) with information of connector IDs and node IDs, as shown in Figure 4.2.

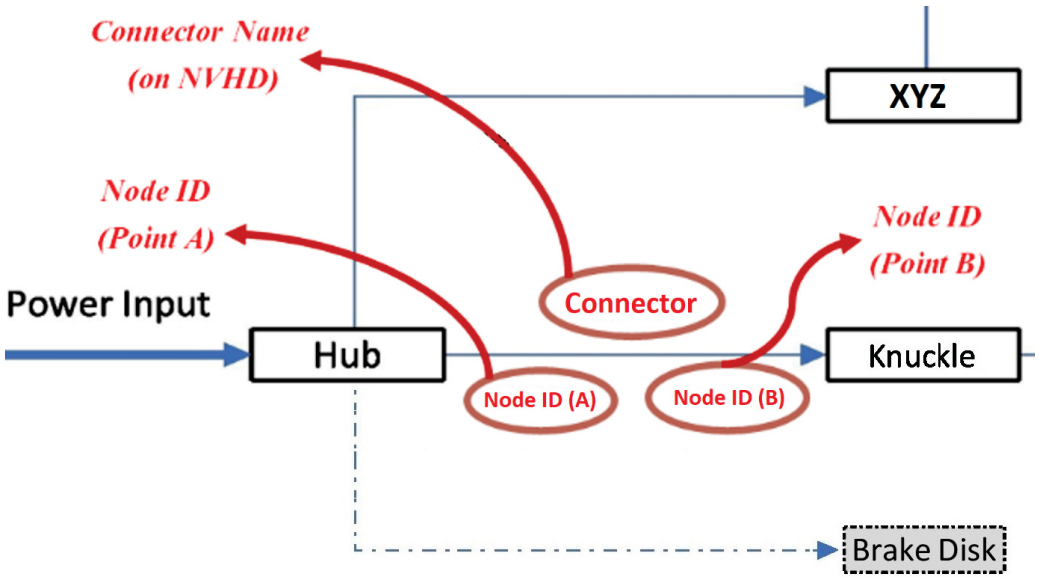

Figure 4.2: Network Representation between wheel hub and suspension

There are some components within the suspension that presumably do not contribute substantially to the power input into trimmed body (for e.g.: hub to brake disk) as they do not have direct connections to any paths leading to trimmed body. These components are boxed in dash-dotted lines and also connected using dash-dotted lines to adjacent components. Other components that are common to the left and right suspension such as Rear Subframe (SubR), etc., are represented using green boxes and their connections are represented to self with green dashed lines.

A detailed network flowchart of suspension representing all the components from hub to trimmed body present on both sides of rear suspension, with their respective connections and connector details is prepared (not shown due to confidentiality). A simplified network flowchart (for easier understanding of connections for readers) consisting of only the connections between a few components (and no connector details) is shown in Figure 4.3. The trimmed body is represented by a grey box to distinguish from other suspension components and is at the centre of flowchart as are the interface points in FEM model. Power is input to the left hub which is connected to many components directly or in-directly such as ERAD (Electric Rear Axle Drive), driveshaft, link arms, Tie Rods, ARB (anti roll bar) through left knuckle. The rear subframe, left spring, left strut, right spring, right spring are the components that connect suspension to body.

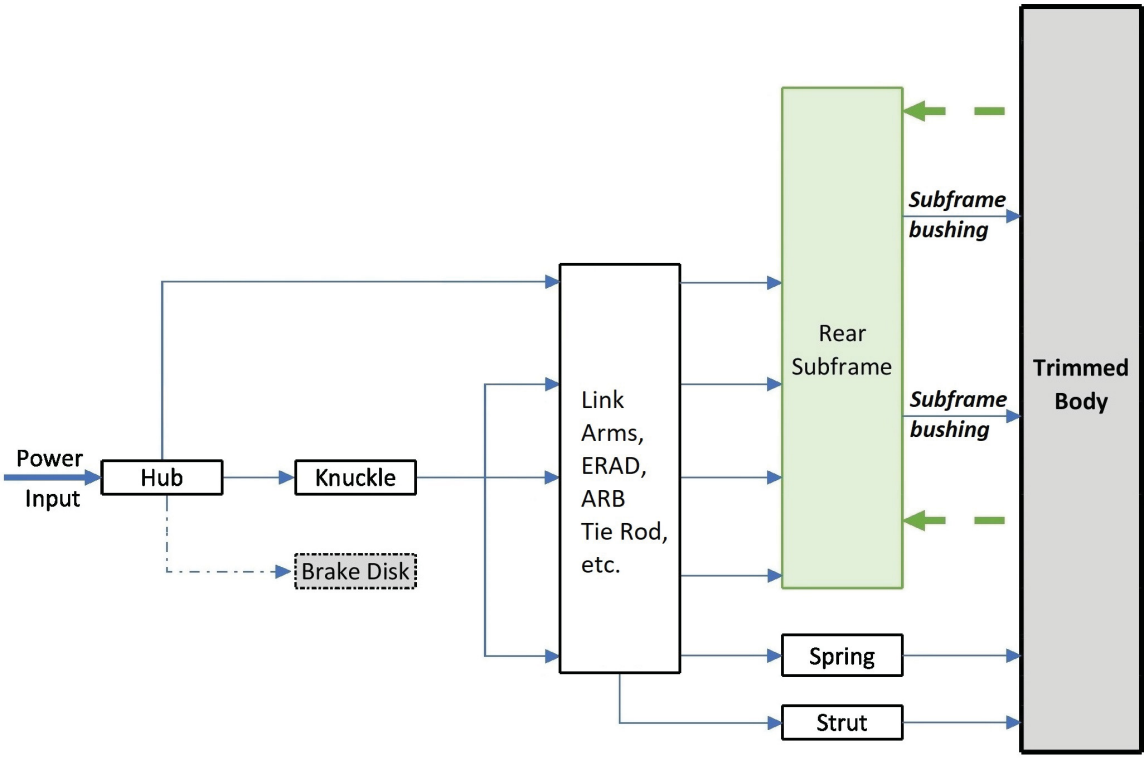

Figure 4.3: Simplified Network Representation of left rear suspension

Figure 4.3 shows the left hand suspension, with connections between hub and trimmed body. Right hand suspension is its mirror image about the trimmed body with the only difference being a lack of power input from right hub.

Chapter 5

Results

5.1 Power Calculations in the Network

The aims of this section are twofold. Firstly - produce results of power flow within the system to develop an understanding of how much and at what frequencies, power is transferred to and from different components. Secondly - restrict the study to fewer transfer paths whose results are extrapolatable and hence can generalized for entire system. This is done by referring to network flowchart produced in previous chapter. This section is planned into three phases for a structured workflow:

1. Firstly, the network diagram is used to identify interface points between suspension and trimmed body. Then nodal forces and velocities are extracted and post-processed in Python/MATLAB to calculate power input to trimmed body from all body interface components. Decision is made on the highest contributing components(s) based on plots produced.

2. Similarly, in the second phase, path is traced back from the highest contributing body interface component(s) to its power input paths. Then, power is calculated from all these paths in the same way as done in Phase I.

3. Lastly, using observation from the first two phases, paths of most relevant components (from the viewpoint of body input power) are charted and a revised network representation is prepared, in order to define the scope of next section of damping study.

5.1.1 Phase I: Power to trimmed body

Trimmed body is connected to the rear suspension at several interface points through 5 interface components which are Rear Subframe, left and right springs, left and right struts. Rear Subframe (SubR) is connected through subframe bushings, left and right springs through connectors each and left and right strut through bushings. The algebraic sum of power exchange through each of these interface points over the entire frequency range provides the net MIP to trimmed body spectrum. Figure 5.1 shows the total MIP to trimmed body, the contribution of each of the five components attached to it, and some important peaks in the spectrum. As can be seen from the plot, there are peaks throughout the spectrum, but the distinct ones are below 200 Hz, and the most distinguished of all is the tire cavity peak at 197Hz.

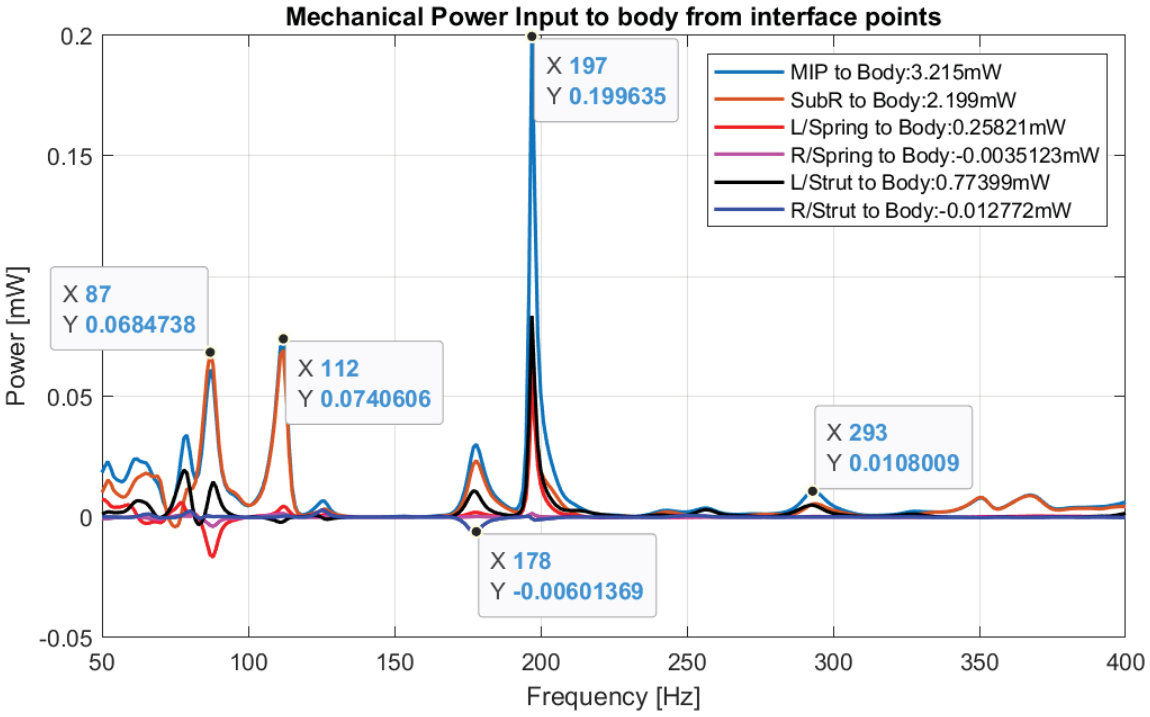

Figure 5.1: Power input to body from the interface components and some important peaks

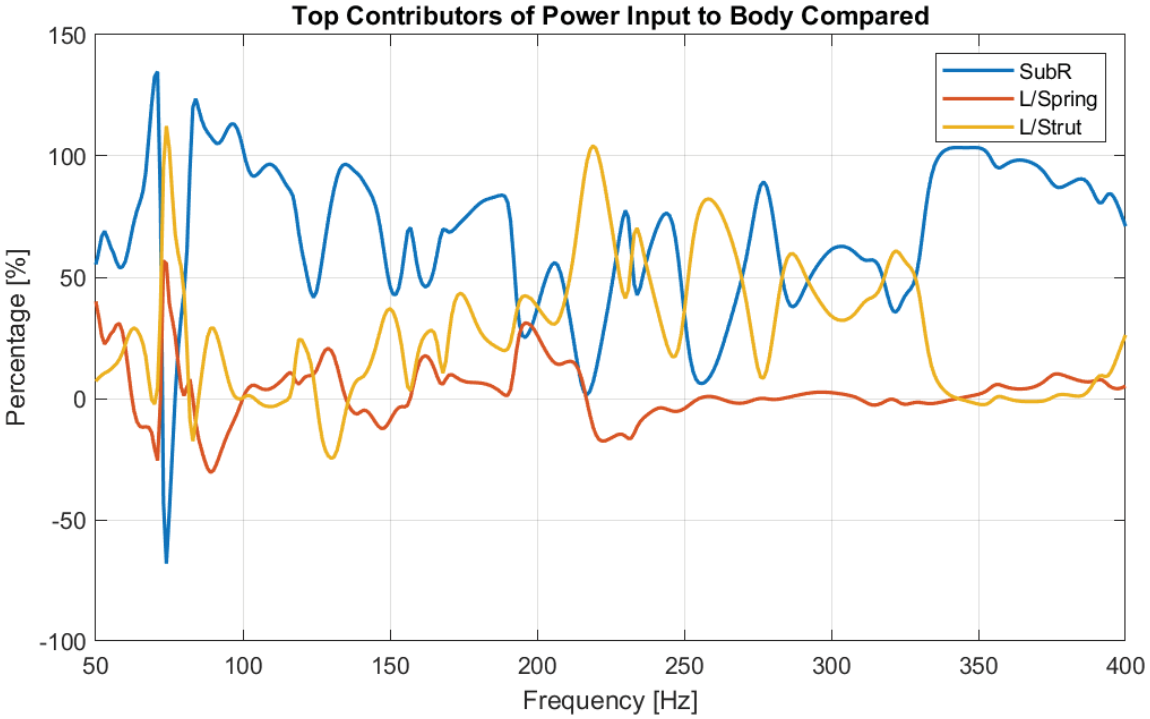

Figure 5.2: Percentage contribution of major contributors to body MIP

In Figure 5.1, rear subframe contributes to about 68% of the total power input to body, whereas left strut and left spring contribute 24% and 8% respectively. These

three turn out to be the top contributors as right strut and spring have a very low and net negative contribution, which means power flows from body into them. This result is somewhat expected, as the load is applied to left tire patch only and no direct load is applied to right hand side suspension.

Figure 5.2 is then produced, showing percentage contribution of top contributors, for a better picture of power contribution to body and stronger decision making on which body interface component(s) can be chosen for the next phase. It is evident from the plots that subframe is the dominant contributor in frequency ranges 82 – 192 Hz and 330 – 400 Hz as it has a positive contribution anywhere between 50% – 100% in these ranges. Left strut has certain dominant peaks but no distinct frequency range where it dominates the power input, whereas left spring is the lowest contributor among the three overall as well as at all frequencies.

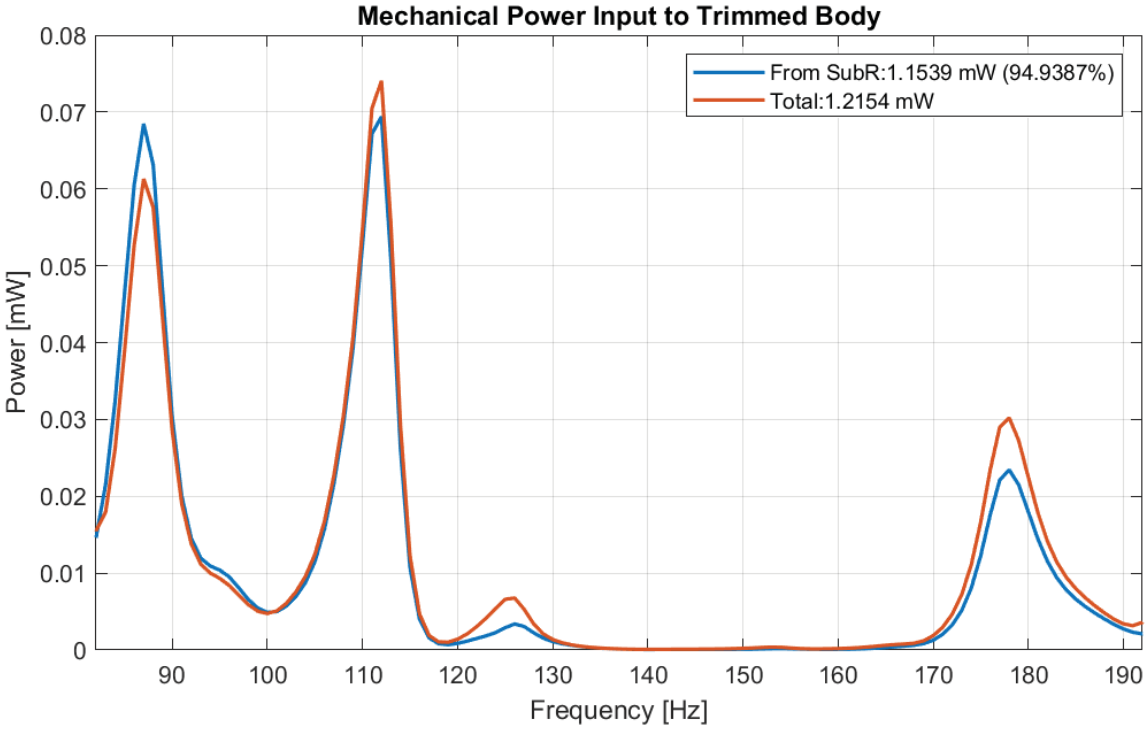

Figure 5.3: Power Input to body from Subframe (82-192 Hz)

Figure 5.3 shows the contribution of subframe towards body MIP, which is in excess of 95% in the frequency range 82 – 192 Hz. From the observations so far, it seems logical to choose only rear subframe in 82 - 192 Hz for further study, as there is an excellent correlation between subframe and trimmed body power in this range. Every change in subframe can be expected to have a direct impact on trimmed body MIP in this range.

In conclusion for this section, rear subframe in the frequency range 82 – 192 Hz is chosen for further analyses as it is presumed to have a very strong link to body MIP. A schematic of interface components that are rejected and accepted for further study, are shown in Figure 5.4

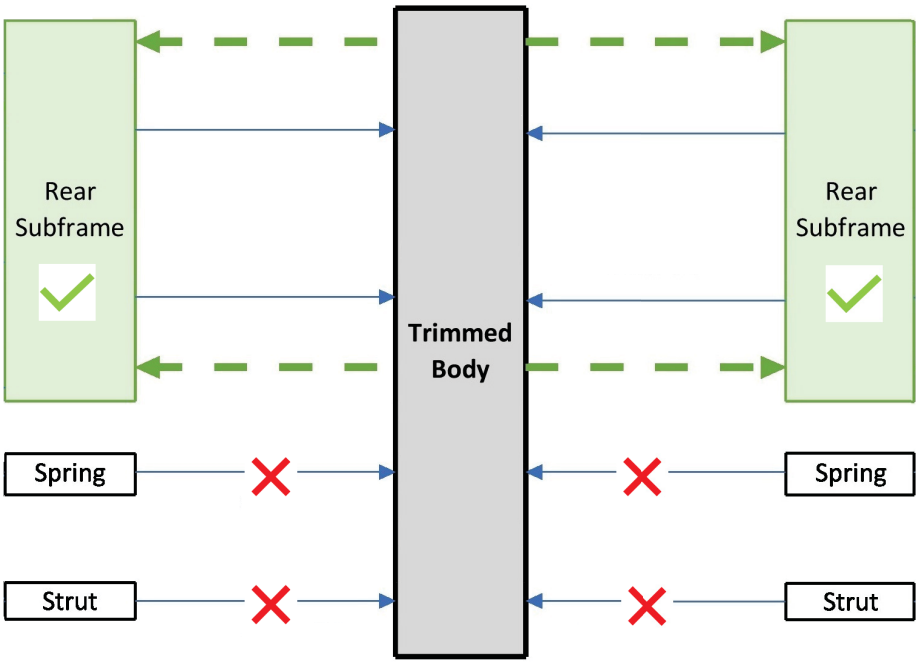

Figure 5.4: Schematic representation of chosen and discarded contributors

5.1.2 Phase II: Power to Body Interface Components

This section deals with investigation of power input to rear subframe from neighbouring components such as links arms, tie rod, etc., which will further narrow down the search for most important path(s).

Rear subframe is connected to several components through one or more points such as:

1. ERAD
2. ARB
3. Left UpLA (upper link arm)
4. Left LoLAF (upper link arm)
5. Left LoLAR (upper link arm)
6. Right UpLA
7. Right LoLAF
8. Right LoLAR

These connections to the rear subframe seem very complex at first glance but can be divided into four different sections as left suspension, right suspension, ERAD and ARB for a simplified understanding. Left suspension consists of the components connecting left knuckle to rear subframe, namely left UpLA, left tie rod, left LoLAF

and left LoLAR. Right suspension consists of respective components connecting right knuckle to rear subframe.

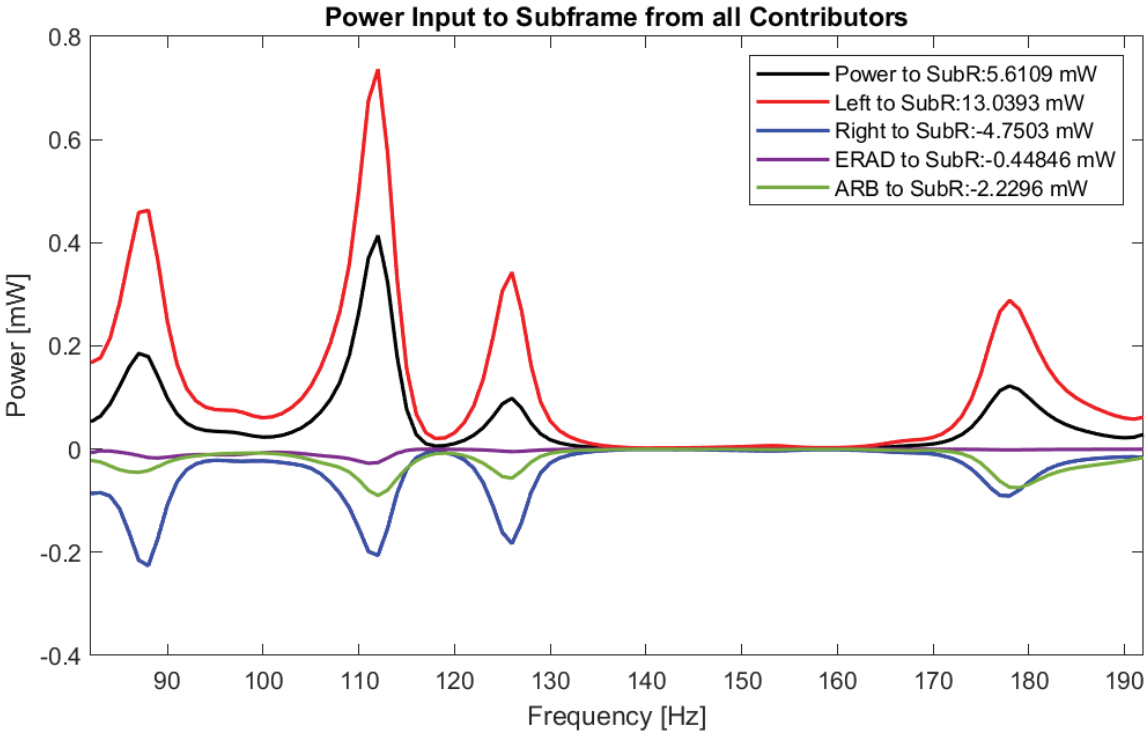

Figure 5.5: MIP to rear subframe from all contributors in 82 – 192 Hz

As concluded in the previous section, this study will be conducted in the frequency range 82 – 192 Hz. So, the algebraic sum of power exchange between subframe and its connected components over this frequency range is calculated, which provides the net MIP to subframe spectrum.

Figure 5.5 shows the total MIP to subframe (= 5.61 mW) plotted with contribution of each of the 4 sections attached to it. Power exchange from ERAD is very small in the low frequencies and close to zero in the mid and high frequencies, hence, the overall contribution (= -0.45 mW) is negative and small enough to be neglected. Similarly, for ARB the overall contribution although higher than that of ERAD, is entirely negative (= -2.23 mW). In case of right suspension, the total power input to subframe (= -4.75 mW) is very high (80% of the net power input to subframe) but negative throughout the spectrum. The only section that provides a positive power input to rear subframe (= 13.04 mW) and hence the only section of interest, is the left suspension. The plots of MIP to subframe and contribution of left suspension have a highly similar trend as can be seen in Figure 5.5. This brings us to a conclusion, that making changes in the left suspension would have considerable impact on the power input to subframe and hence trimmed body.

Figure 5.6 shows the breakdown of each component's contribution from right suspension to the rear subframe. All the components have an entirely negative power spectrum except one positive peak of right UpLA because of its complex connections to both sides of suspension through ARB.

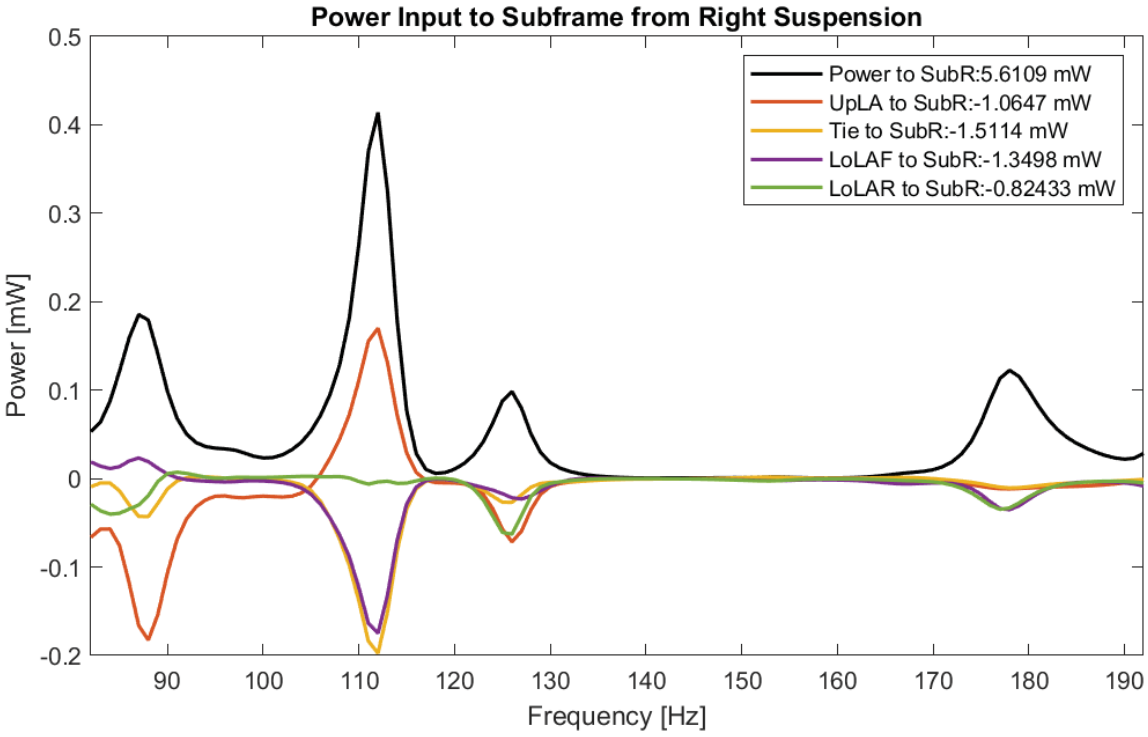

Figure 5.6: MIP to rear subframe from right suspension in 82 – 192 Hz

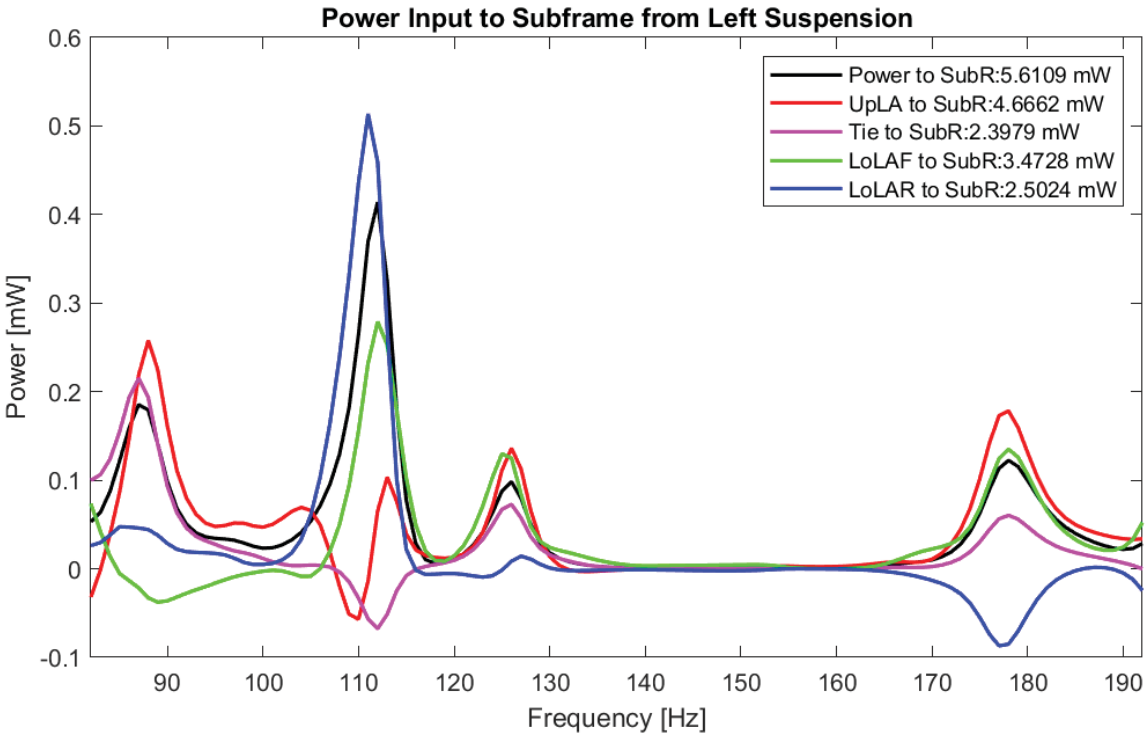

Figure 5.7: MIP to rear subframe from left suspension in 82 – 192 Hz

As mentioned earlier, the only section of interest now is the left suspension and Figure 5.7 shows the breakdown of each component's contribution from left suspension to the rear subframe's MIP. All the components have substantial contribution

towards subframe power input, but the connections of left UpLA and left LoLAR are quite complex, as left UpLA is connected to right UpLA through ARB and another component (not written due to confidentiality), whereas the motion of left LoLAR is highly dependent on its connections to left spring and left strut.

To be able to draw strong conclusions from damping study, it is crucial that the path(s) chosen is as independent as possible and any alterations to its damping properties have direct impact on the MIP of subframe and hence body. Therefore, the relevant components in left suspension need to be narrowed down to left Tie Rod and left LoLAF as they contribute greatly to the power input to rear subframe and also have direct connections to subframe.

In conclusion, the paths connecting left Tie Rod and left LoLAF to trimmed body through subframe are considered for further study, whereas the contribution of left UpLA, left LoLAR, right suspension, ERAD and ARB are neglected for further study.

5.1.3 Phase III: Conclusions from Power Study and Revised Network Flowchart

A revised network is prepared in this section based on conclusions drawn on most relevant paths that affect MIP to trimmed body, from Phase I and Phase II observations. The purpose of this exercise is to list out explicitly the path that will be studied in later sections. So, revised network should contain the components as well as connector details from NVHD (not shown due to confidentiality) to design experiments around them.

Revised network representation should have paths that consist of left suspension's tie rod and LoLAF and their connections to trimmed body through rear subframe. A simplified revised flowchart is prepared as shown in Figure 5.8 (Detailed flowchart is not shown due to confidentiality). Components like left knuckle and left hub are only indicative of the source of power flow in the flowchart. They are not included in power calculations and will not be used in damping study for the same reason as discussed in previous phase for left UpLA and left LoLAR, that their complex connections might interfere with behaviour of other components and in turn make it difficult to draw final conclusions based on the left Tie rod and left LoLAF.

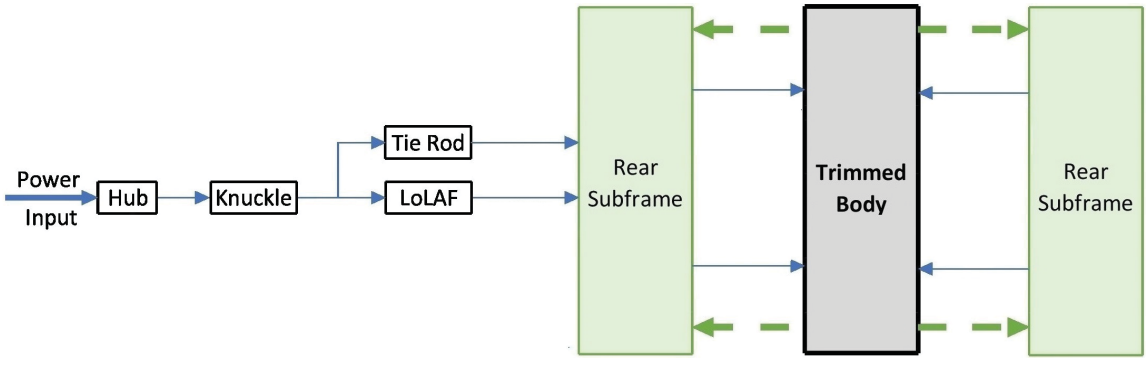

Figure 5.8: Revised network flowchart

5.2 Correlation between Mechanical Input Power and Noise

Power calculations in previous section were aimed at identifying paths within the suspension network that have strong relationship with trimmed body in terms of MIP. This chapter acts as a bridge between power calculations and damping study. It deals with cabin sound pressure calculations and develops a method of correlating body MIP and cabin noise. To do so, the model is provided with 4 mics on occupants' ear locations as shown by an example in Figure 5.9. Data from these mics are used for further analysis.

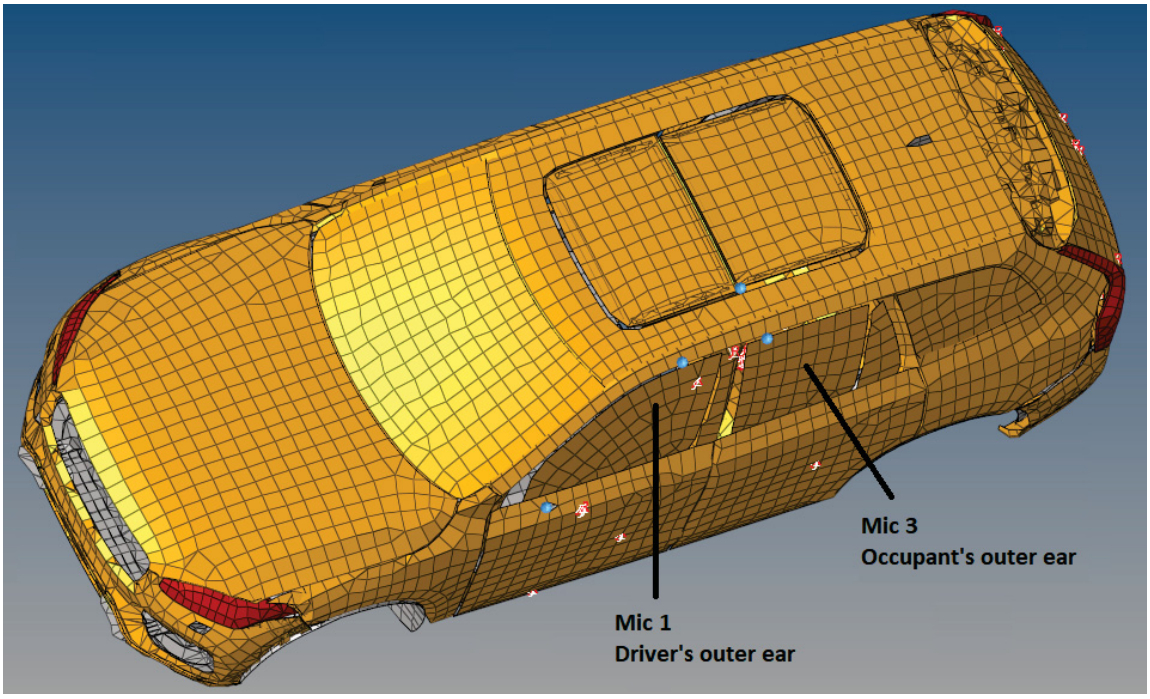

Figure 5.9: Example of Mic 1 and 3 locations in a trimmed body model

5.2.1 Interior Noise Calculations

This section is focussed on calculation of average acoustic pressure (Equation 2.114) within the cabin obtained from all four mics, positions of which are shown in Figure 5.9. Averaged sound pressure in the entire frequency spectrum in dB scale is plotted in Figure 5.10.

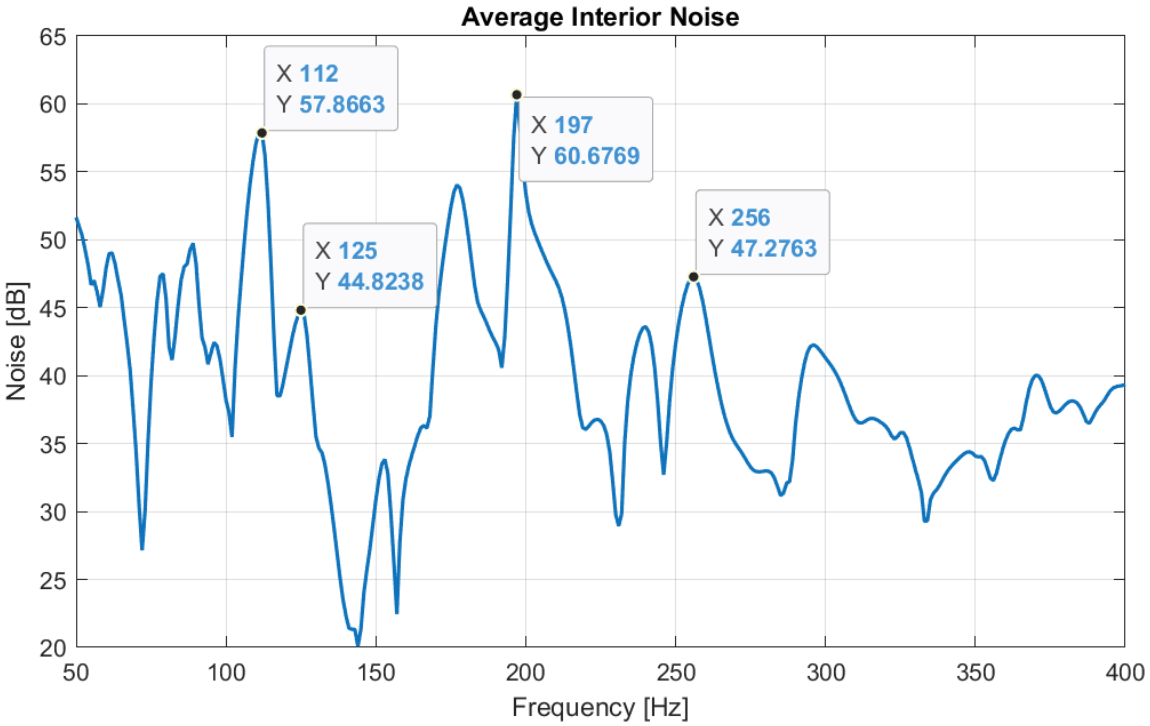

Figure 5.10: Average SPL in the entire spectrum in dB scale

The maximum sound pressure level (SPL) is about 60 dB obtained at 197 Hz, the cavity peak frequency. SPL values are within expected range of interior noise levels and most peaks in spectrum are observed at same frequencies as in body MIP spectrum, which points at a good relation between MIP and SPL.

5.2.2 Results

This section is focussed on developing ways of studying the correlation between body MIP and SPL. For an all-round study of MIP and SPL relation, it is important to firstly compare them graphically, and then mathematically. Mathematical comparison can be done by defining an indicator that acts as a measure of their correlation.

MIP and SPL are two different physical quantities having units of power and pressure, hence a logic needs to be developed to be able to graphically study their correlation. Now, it is worth noting that decibel values for quantities with squared units (Let, A^2) or power spectra are calculated using the following relation:

$$A_{dB} = 10log_{10}(A/A_0) \tag{5.1}$$

Whereas, decibel values for other quantities (Let, B) are calculated using the following relation:

$$B_{dB} = 20log_{10}(B/B_0) \tag{5.2}$$

where, A_0/B_0 is the reference value of quantity A/B. Hence, to study the correlation between MIP and SPL values, a preliminary idea could be to compare the values of SPL^2 with MIP, since SPL is a quantity like B and MIP like A.

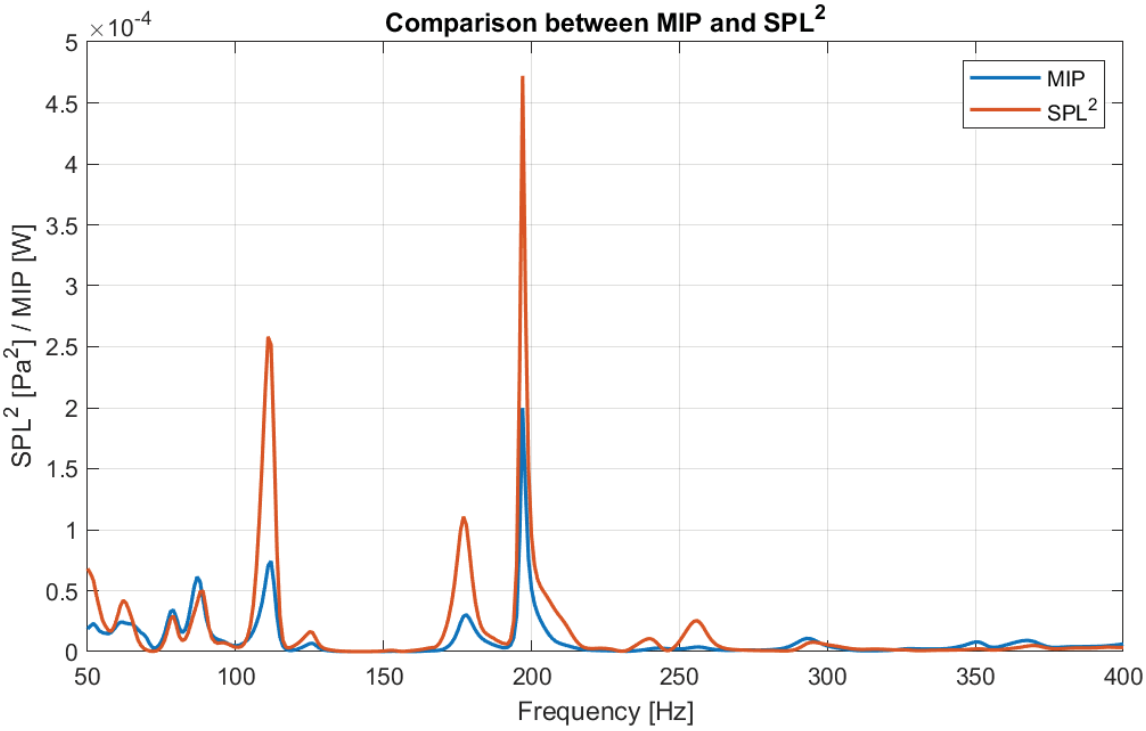

Figure 5.11: SPL^2 compared with MIP in frequency range 50 – 400 Hz

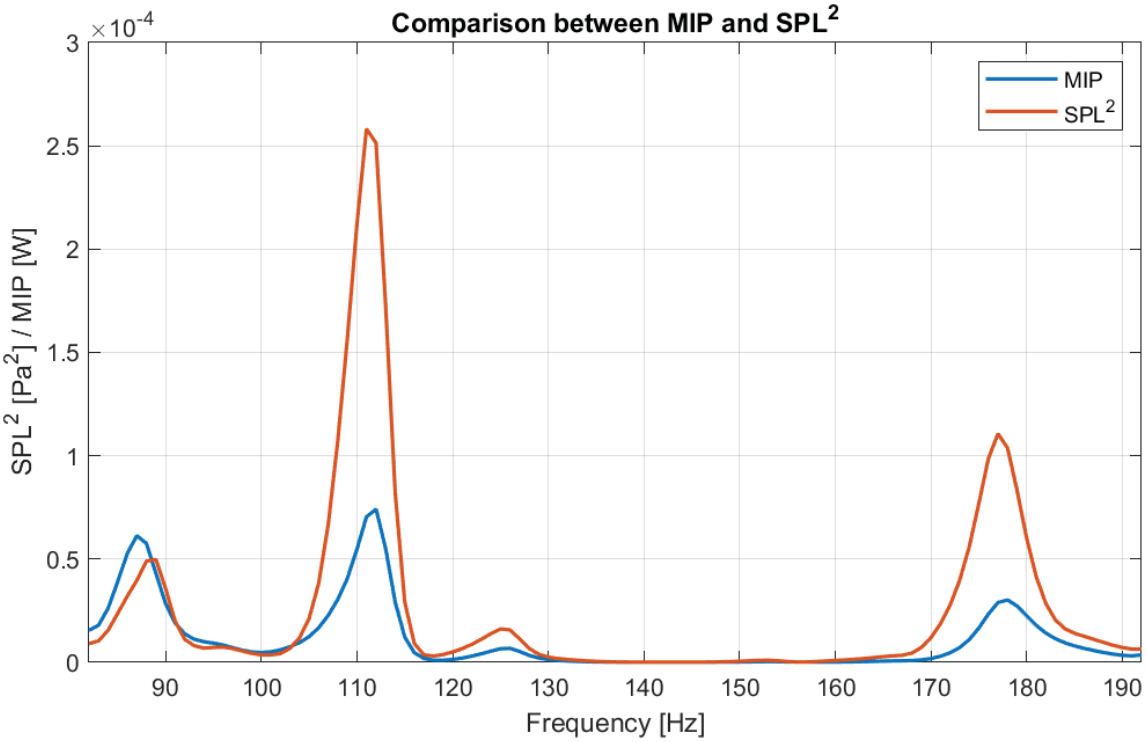

Figure 5.12: SPL^2 compared with MIP in frequency range 82 – 192 Hz

Figure 5.11 and 5.12 show plots comparing MIP and SPL^2 against frequency and the correlation between them appears very strong. Every peak of one quantity follows

the other. This analysis shows that the idea behind comparison of MIP and SPL^2 is a good direction for this study, but it needs to be followed with more concrete mathematical relation. So, to build up on the idea of establishing a mathematical indicator relating SPL^2 with MIP, the following expression can be studied:

$$SPL^2 = T(f) * MIP \tag{5.3}$$

Where, $T(f)$ is like a transfer function with MIP as input and SPL^2 as response. It can be used as the mathematical indicator to study their correlation as it provides the ratio of their magnitudes in SI units. For example, if the relation between MIP and SPL is perfect, then $T(f)$ would have a constant value throughout the frequency range, or in words the standard deviation of $T(f)$ would be zero.

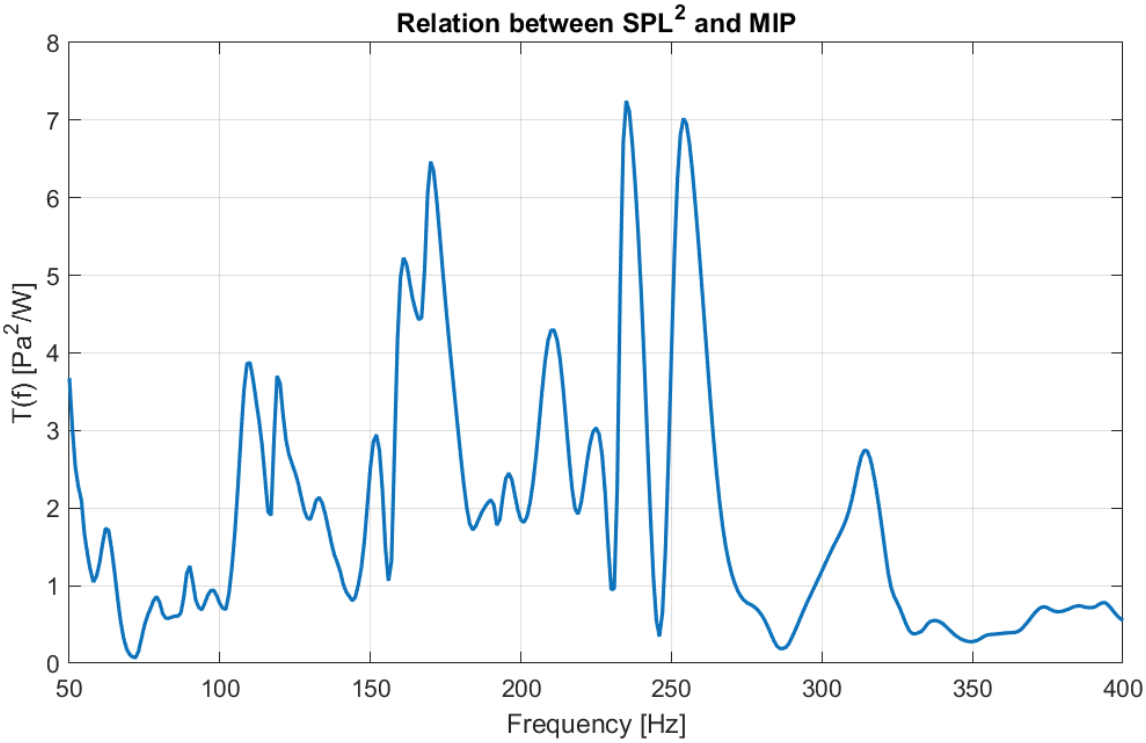

Figure 5.13: T(f) plot for frequency range 50 – 400 Hz

Transfer function $T(f)$ is plotted against frequency in the range 50 – 400 Hz as given in Figure 6.5, where its values lie within 7 units. $T(f)$ shows a linearly increasing trend in the frequency range around 75 – 225 Hz. Since, the chosen frequency range for study, 82 – 192 Hz lies within it, damping study in later sections can be focussed in this range that compares values of $T(f)$ for different damping cases.

5.3 Impact of Damping

After the relation between MIP and interior noise in developed, this concluding chapter deals with studying the impact of different modelling of damping within the chosen suspension paths on the MIP, SPL and their relation, by basing the study on a set of design of experiments (DOEs) applicable to pre-decided transfer paths and frequency ranges.

5.3.1 Damping models

The two types of damping models to be used for studying impact of damping in this dissertation, are the viscous and structural damping models. Parameter used to define structural damping within a system is loss factor (η) and viscous damping in a system is defined by either damping coefficient (c) or damping ratio (ζ).

For an analysis like in this section, where different damping models are compared, it is crucial to compare equivalent values of damping parameters corresponding to each model (and not just random damping values), to draw strong conclusions. For example, in this dissertation, where viscous and structural damping models are to be compared, it must firstly be identified which equivalent viscous damping parameter (c_{eq} or ζ_{eq}) should be compared to structural damping loss factor (η). Here, this choice is driven by what input does the software accept for defining viscous damping within a system.

Now, according to documentation of Altair Optistruct, the software uses damping coefficient c as input for viscous damping parameter. So, equivalent relation between structural and viscous damping for an element, that can be used to obtain values for comparison (derived in Section 2.6.2), is given as:

$$c_{eq} = \frac{\eta k}{\omega} \tag{5.4}$$

Where, c_{eq} is the equivalent viscous damping coefficient corresponding to structural damping loss factor η, and k is the stiffness of element. Since, the frequency range of interest is $82 - 192Hz$, the frequency at which equivalent viscous damping needs to be calculated is preferred between the frequency range at $126Hz$ (as the structure has a considerable response at $126Hz$, seen in Figure 5.12). This can help capture relevant effects at high as well as low frequency withing the range. Now, putting the value of $\omega = 2\pi f = 2\pi * 126Hz$, equivalent viscous damping is calculated for this study.

5.3.2 Design of Experiments

In this subsection, a set of DOEs are prepared to investigate influence of high and low damping ratios, types of localization of damping, modelling of damping, etc. Hence, the DOEs are so constructed that they deal with extreme cases of damping, such that the effect of different damping scenario can be observed with ease. It is to be noted that these DOEs are applied only to the connectors and components in chosen transfer paths and frequency range 82 - 192 Hz as stated in previous chapter.

Table 5.1: DOEs for Damping Study

Exp Nr.	Experiment Description	Damping Coefficient/ Loss Factor
1	Baseline – original damping case	$\eta_{bush} = 0.05$ $\eta_{component} = 0.08$
2	5% structural damping localized into connectors	$\eta_{bush} = 0.05$
3	Viscous damping equivalent to 5% structural damping localized into connectors	$c_{bush} \equiv \eta_{bush} = 0.05$
4	25% structural damping localized into connectors	$\eta_{bush} = 0.25$
5	Viscous damping equivalent to 25% structural damping localized into connectors	$c_{bush} \equiv \eta_{bush} = 0.25$
6	8% structural damping localized into components	$\eta_{component} = 0.08$
7	40% structural damping localized into components	$\eta_{component} = 0.4$

First DOE is the calculation model in its original state of damping (generalized structural damping of 5% in suspension bushings and 8% in suspension components). For second DOE, 5% structural damping is localized into bushings and no damping is in the components. For third DOE, viscous damping (equivalent to 5% structural damping) is localized into bushings and no damping is in the components. For fourth DOE, very high structural damping of 25% (5 times the nominal value of 5%) is localized into bushings and no damping is in the components. For fifth DOE, very high viscous damping (equivalent to 25% structural damping) is localized into bushings and no damping is in the components. In sixth DOE, 8% structural damping is localized into components and no damping is in the bushings. In final DOE, very high structural damping of 40% (5 times the nominal value of 8%) is localized into components and no damping is in the bushings. So, the DOE 2 to 5 deal with localizing viscous and structural damping into connectors (bushings), whereas DOE 6 and 7 deal with localizing structural damping into components.

5.3.3 Effects on Power and Noise

This section deals with results of DOEs obtained in terms of MIP, SPL and $T(f)$.

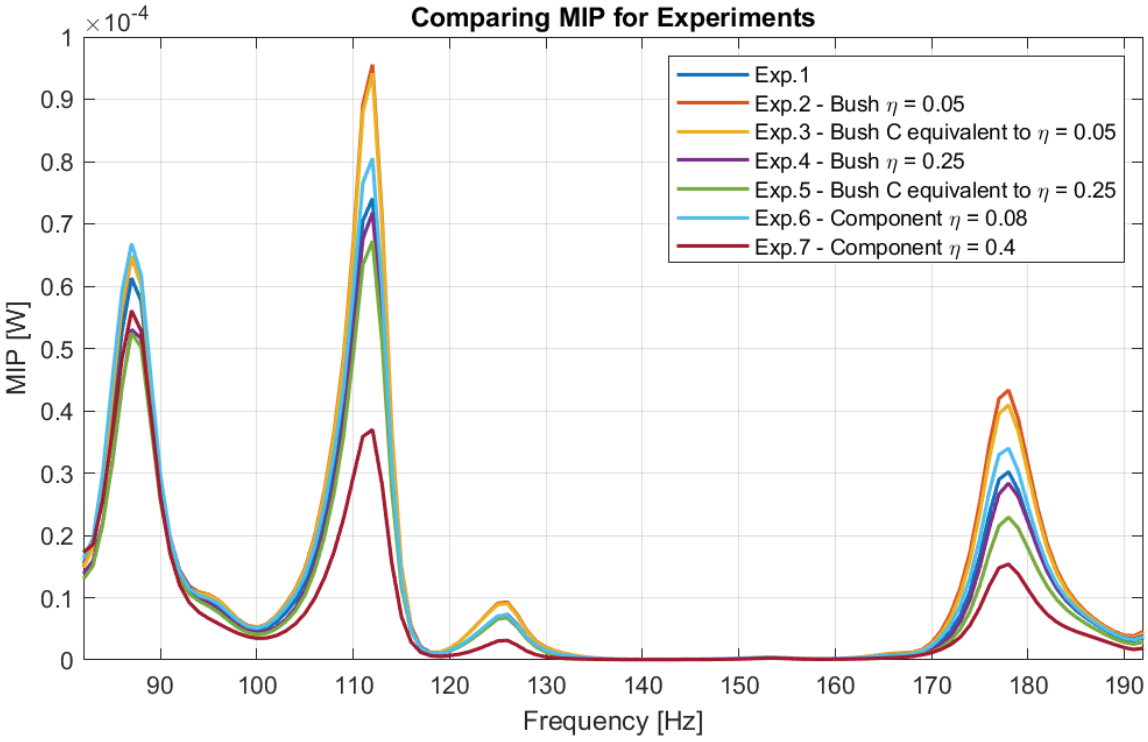

Figure 5.14: MIPs compared for all Experiments in range 82 – 192 Hz

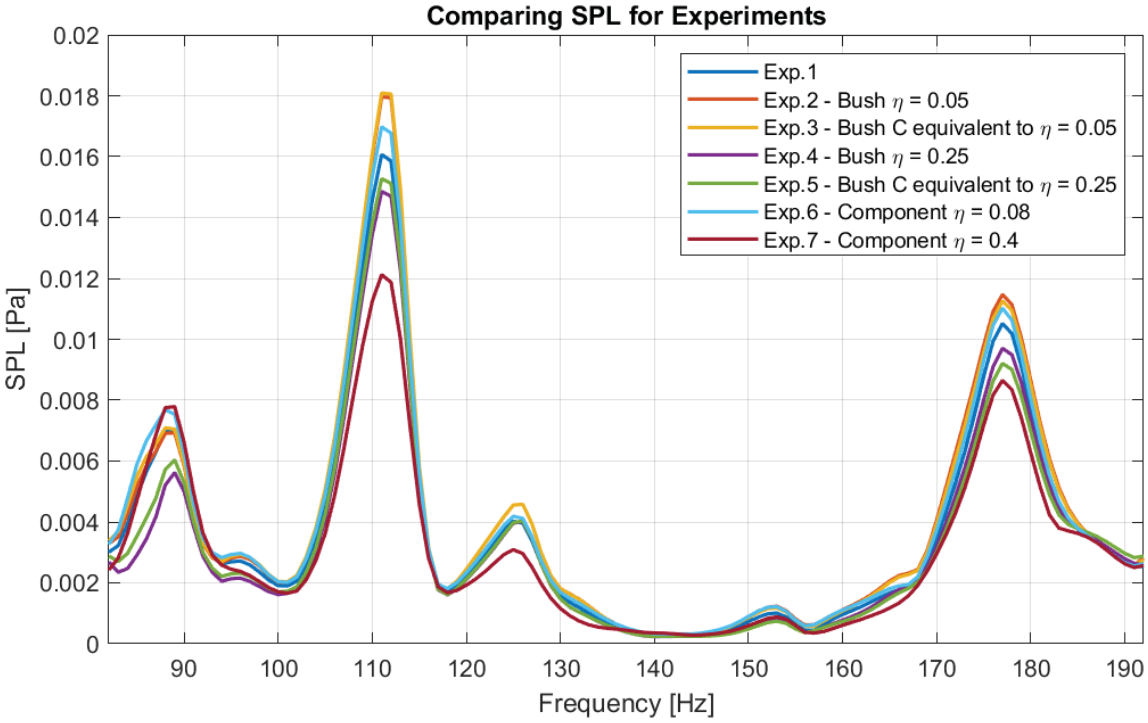

Figure 5.15: SPLs compared for all Experiments in range 82 – 192 Hz

Figure 5.14 and 5.15 show plots comparing body MIPs and average cabin SPLs respectively for all experiments. At a first glance, experiment 2 with 2.5% structural damping localized into bushings seems to show the highest power and SPL throughout the frequency range, and experiment 7 with 40% structural damping localized into components has the lowest power and SPL almost in the entire frequency range. Experiment 3 has the second highest response whereas all other have responses that lie between results of 2 and 7 for both MIP and SPL, without a clear difference between the response levels. These results also confirm the good agreement between body input power and cabin sound pressure levels.

Based on results obtained for MIPs and SPLs for all experiments (in Figure 5.14 and 5.15), it is evident that increasing value of damping results in a decrease MIP and hence SPL values. There seems to be a great agreement between the rate of change in MIP and SPL values.

5.3.4 Effects on relation between Power and Noise

After obtaining results of damping effect on MIP and SPL, the impact on their relation T(f) needs to be studied. But, before obtaining values of T(f), a method of interpreting the results of T(f) needs to be identified such that the quality of correlation of MIP and SPL can be judged. Since, T(f) is a ratio of SPL^2 and MIP, an ideal system with the best correlation will have a constant value of T(f). So, the quality of their correlation can be judged by calculating the amount of variation or deviation of T(f) from its mean value. A measure of it is the standard deviation of T(f). So, calculating the standard deviation of T(f) can be directly related to the quality of correlation of SPL and MIP, such that higher the standard deviation, poorer is the correlation and vice versa. Standard deviation of T(f) can be calculated by taking the following steps.

Firstly, considering that there are n data points in the frequency range, mean μ of the transfer function is calculated using formula:

$$\mu = \frac{T(f_1) + T(f_2) + \ldots + T(f_n)}{n} \tag{5.5}$$

Now, the variance σ^2 is calculated by taking the mean of square of deviation of all data points as given by the equation:

$$\sigma^2 = \frac{(T(f_1) - \mu)^2 + (T(f_2) - \mu)^2 + ... + (T(f_n) - \mu)^2}{n} \tag{5.6}$$

Where, σ is the standard deviation and can be calculated by taking the square root of variance. Or,

$$\sigma = \sqrt{\frac{(T(f_1) - \mu)^2 + (T(f_2) - \mu)^2 + ... + (T(f_n) - \mu)^2}{n}} \tag{5.7}$$

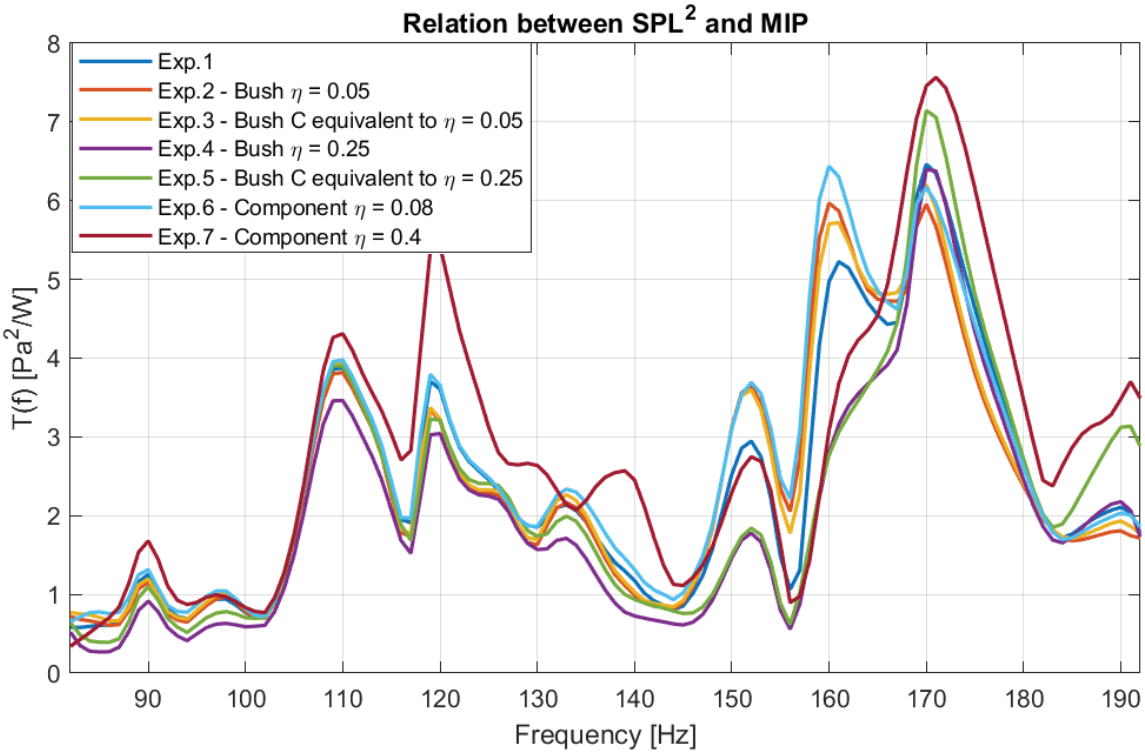

Figure 5.16: Plot of T(f) in frequency range 82 – 192 Hz

Table 5.2: Standard deviation of $T(f)$

Exp.Nr.	Experiment Description	Standard Deviation
1	Baseline – original damping case	1.496
2	5% structural damping localized into connectors	1.483
3	Viscous damping equivalent to 5% structural damping localized into connectors	1.478
4	25% structural damping localized into connectors	1.407
5	Viscous damping equivalent to 25% structural damping localized into connectors	1.526
6	8% structural damping localized into components	1.555
7	40% structural damping localized into components	1.731

Figure 5.16 shows comparison between T(f) for all experiments. Standard deviation of T(f) in frequency range $82 - 192Hz$ is calculated (and presented in Table 5.2) for better interpretation of results. Conclusions will be drawn on two parameters namely standard deviation of $T(f)$ and how it changes with an increase in the damping value.

It is observed that standard deviation is the least for damping case where structural damping is localized into bushings (experiment 2 and 4), and it decreases with an increase in the value of loss factor. This can also be validated in Figure 5.16, where experiment 4 has the most uniform graph as observed visually, owing to smaller peaks (at many frequencies) or flattened peaks (around 158 Hz). Viscous damping localized into bushings (Experiment 3 and 5) have similar standard deviation level but

they increase with increased damping value. Structural damping localized into components (experiment 6 and 7) has a similar behavior to experiment 3 to 5, as its standard deviation increases with increasing damping values.

Based on results obtained for T(f), it can be concluded that:

1. **Structural damping localized into connectors**: The correlation between MIP and SPL improves with an increase in the value of loss factor.

2. **Viscous damping localized into connectors**: The correlation between MIP and SPL deteriorates with an increase in the value of loss factor.

3. **Structural damping localized into components**: The correlation between MIP and SPL deteriorates with an increase in the value of loss factor.

In conclusion, structural damping localized into bushings show better correlation between MIP and SPL with increasing damping values, and seems to capture damping losses better than other damping cases.

5.3.5 Active and Reactive Power

Active power is the cycle averaged power that corresponds to the real part of complex power and is the power that is dissipated due to damping present within system. Imaginary part of complex power is the reactive power that causes standing waves withing structure. Although reactive power is assumed irrelevant to the study according to [5], to instil confidence in the chosen "active power" for this study, a check is conducted in this section that compares correlation between:

Case 1: interior noise − active power

Case 2: interior noise − reactive power

in the entire frequency spectrum, i.e., 50 – 400 Hz.For the comparison to be conclusive, firstly, plot between SPL^2 and MIP is compared for both cases. The baseline experiment or experiment 1 with original system damping parameters is used for this comparison. Secondly, T(f) is compared for both cases. Results of all seven experiments in DOE are used to draw conclusions for this comparison.

Figure 5.17 and 5.18 show comparison between SPL^2 and MIP for case 1 and 2 respectively. The correlation between active as well as reactive power and SPL looks very similar, but on a closer look the differences can be spotted. Focussing on peaks between 100 and 200 Hz, interior noise seems to show a better correlation with active power than reactive power. SPL^2 shows a proportional change with active MIP for peaks at 111 Hz, 125 Hz, 177 Hz and 197 Hz. Whereas, reactive MIP overshoots SPL^2 in the peak at 125 Hz. The sizes of reactive MIP peaks at 111 Hz and 177 Hz are similar but those of SPL^2 differ by about 50%. Additionally, in the frequency range between 300 – 400 Hz, SPL^2 follows the plot of active power much better in relation to reactive power, which appears to have an extra peak around 330 Hz.

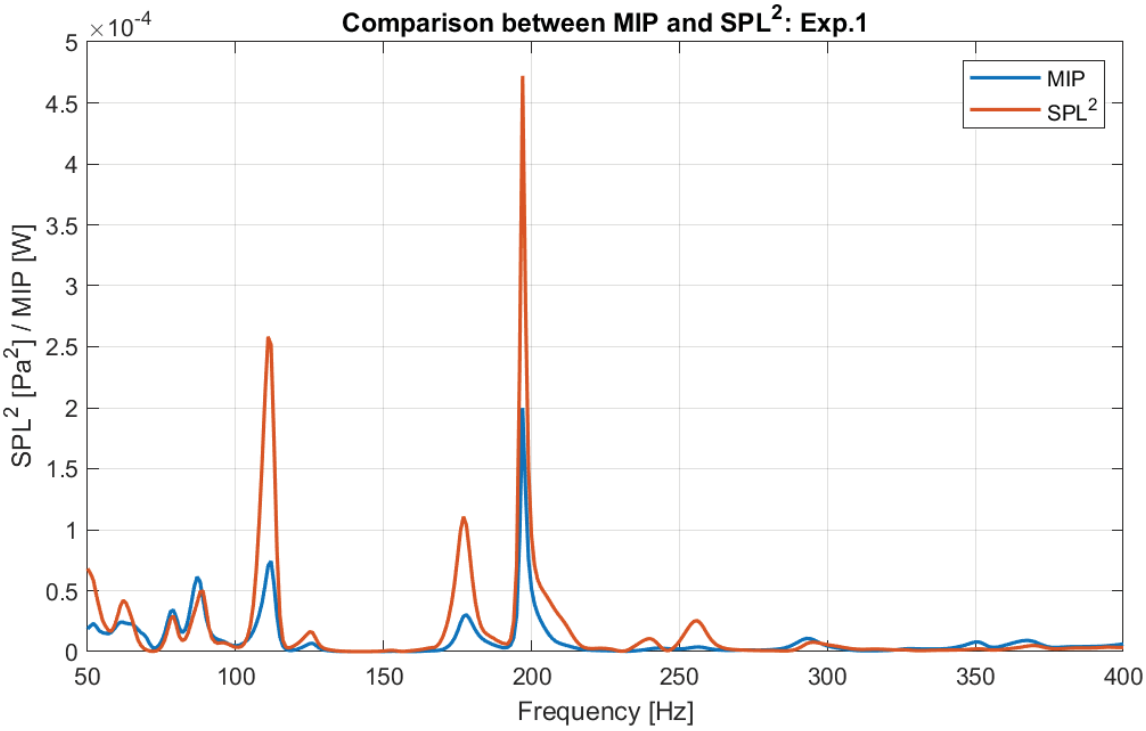

Figure 5.17: Plot of Active power and Interior Noise showing their correlation

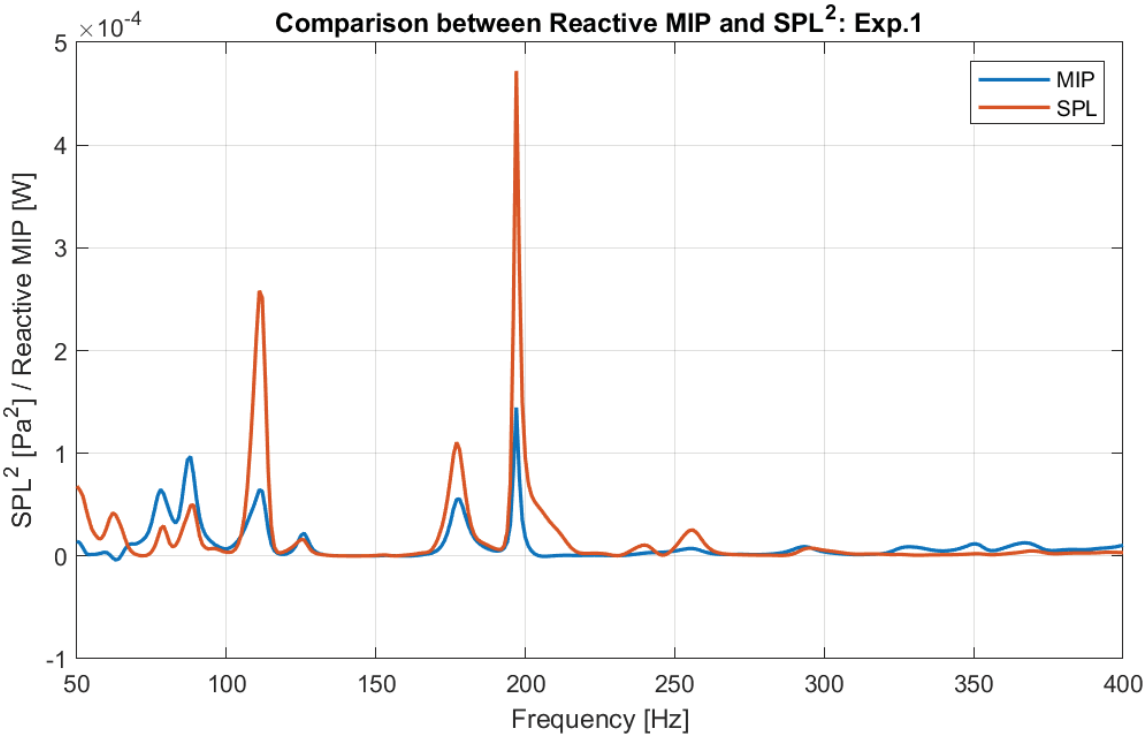

Figure 5.18: Plot of Reactive power and Interior Noise showing their correlation

Now, that active and reactive MIPs of experiment 1 are compared based on their correlation to SPL^2, plots of $T_{active}(f)$ and $T_{reactive}(f)$ are produced for all seven experiments to draw robust conclusions for this comparison.

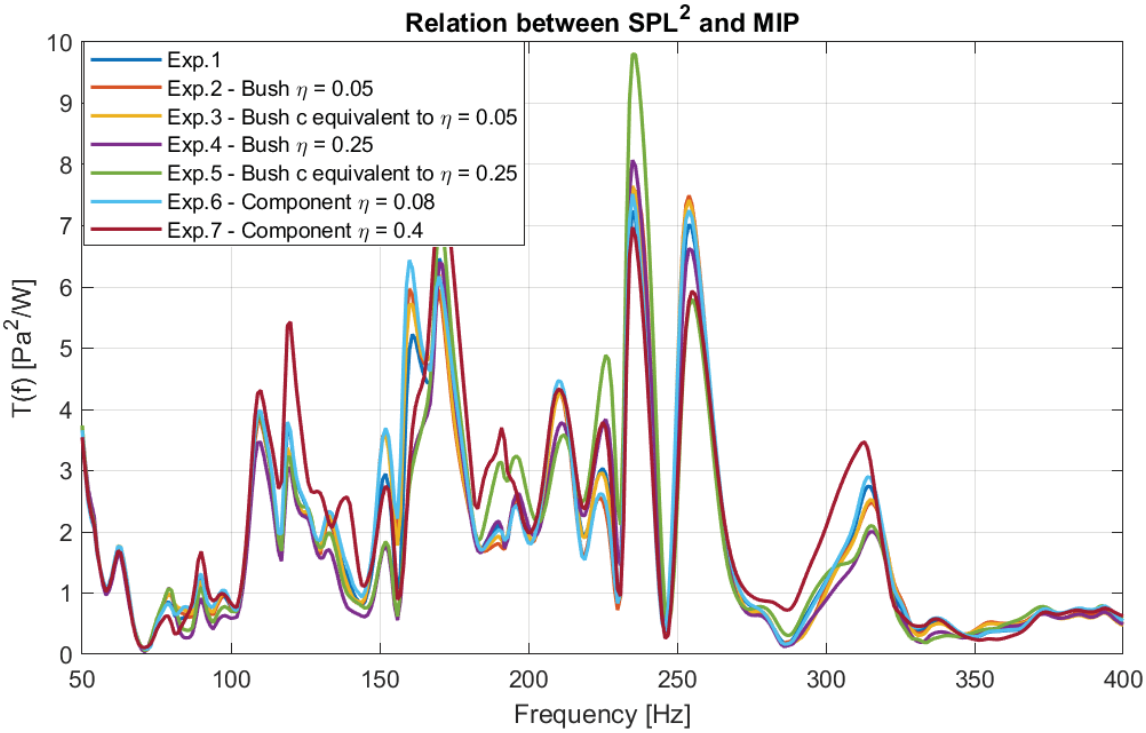

Figure 5.19: Plots of active T(f) for all experiments

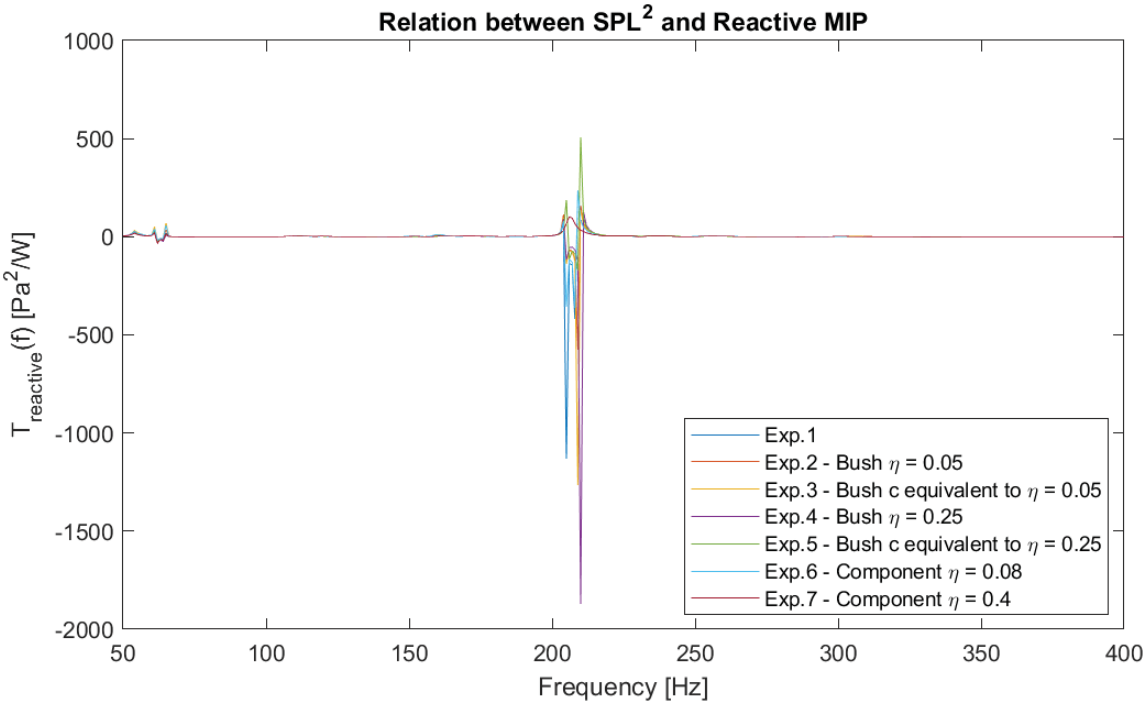

Figure 5.20: Plots of Reactive T(f) for all experiments

where,

$$T_{active}\,(f) = \frac{SPL^2}{MIP_{active}} \tag{5.8}$$

$$T_{reactive}(f) = \frac{SPL^2}{MIP_{reactive}} \tag{5.9}$$

As discussed in previous chapter, lesser the variation in value of transfer function T(f), better is the correlation between SPL and MIP. Figure 5.19 and 5.20 show that value of $T_{active}(f)$ stays within 0 to 9 units whereas $T_{reactive}(f)$ varies between 200 to -2000 units in the entire spectrum.

The values of $T_{reactive}(f)$ are similar or slightly higher to $T_{active}(f)$ in most of the frequency spectrum and much higher than in others, especially around 50 – 70 Hz, 200 – 210 Hz, etc. This results in a clear victory for active MIP, or in other words the correlation between SPL^2 and active MIP is much better than that of reactive MIP, which means the chosen active power is indeed relevant to the study and is the power that contributes to production of interior noise.A

5.3.6 Body damping cases

Damping within suspension has shown to have a direct impact on mechanical input power and interior noise, but no frequency dependence is observed in system response by changing damping models. Additionally, the impact of varying damping within suspension on interior noise is not as high as expected, which raises the question of impact of damping within trimmed body and cavity fluid on the interior noise. A set of DOEs is prepared to study the influence of trimmed body damping and cavity damping on MIP and interior noise as given in table below:

Table 5.3: DOEs for studying impact of trimmed body damping and cavity damping

Exp.	Experiment Description
1	Baseline – original damping case
2	Equivalent structural damping in Trimmed Body
3	Trimmed body damping = 0
4	Trimmed body damping = 0 and Cavity damping = 0

First DOE is the calculation model in its original state of damping. For second DOE, equivalent structural damping is modelled into trimmed body. For third DOE, damping in trimmed body is set to zero. For final DOE, trimmed body damping as well as damping within cavity fluid is set to zero.

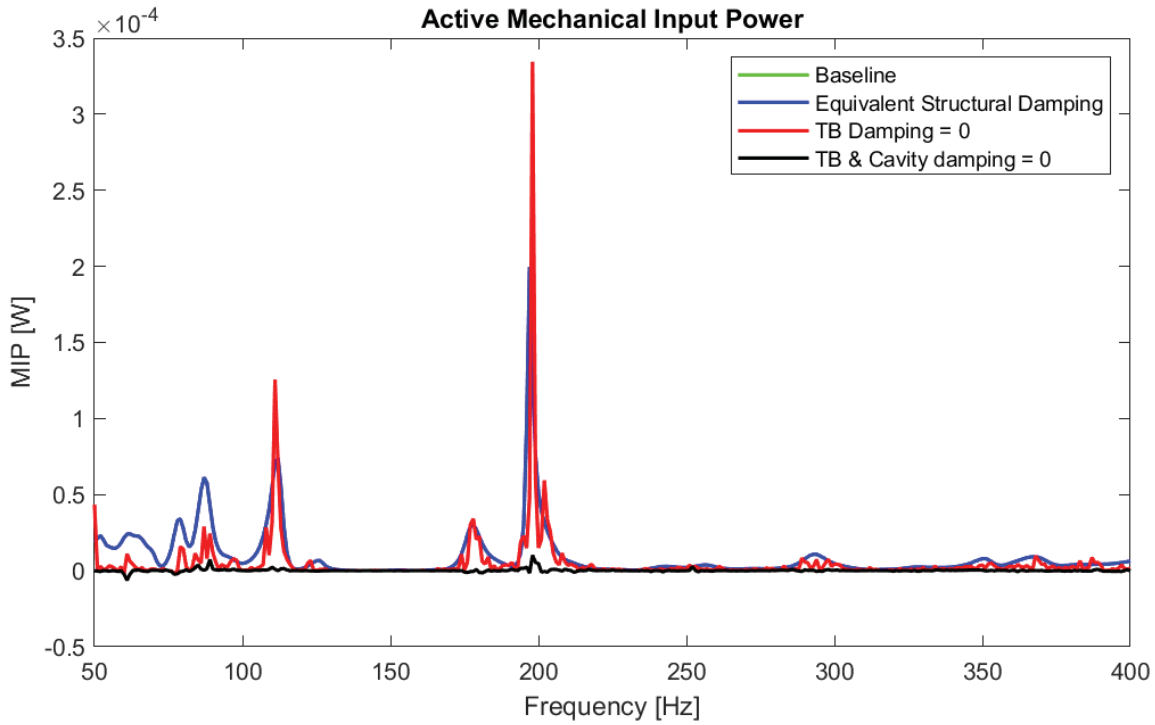

Figure 5.21: Active MIP for all 4 experiments

Figure 5.21 shows the active MIPs compared for all 4 experiments and it is observed that equivalent structural damping (<experiment 2) produces same result as baseline

case. Additionally, for experiment 3, where damping in trimmed body is removed, the cavity peak obtained is about 70% higher compared to baseline and the response is very erratic with random high and low responses throughout the spectrum. The most interesting result however is of experiment 4, which suggests that active MIP reduces to less than 5% of baseline, when the cavity damping is put to zero. This suggests an important role played by cavity fluid damping in input power.

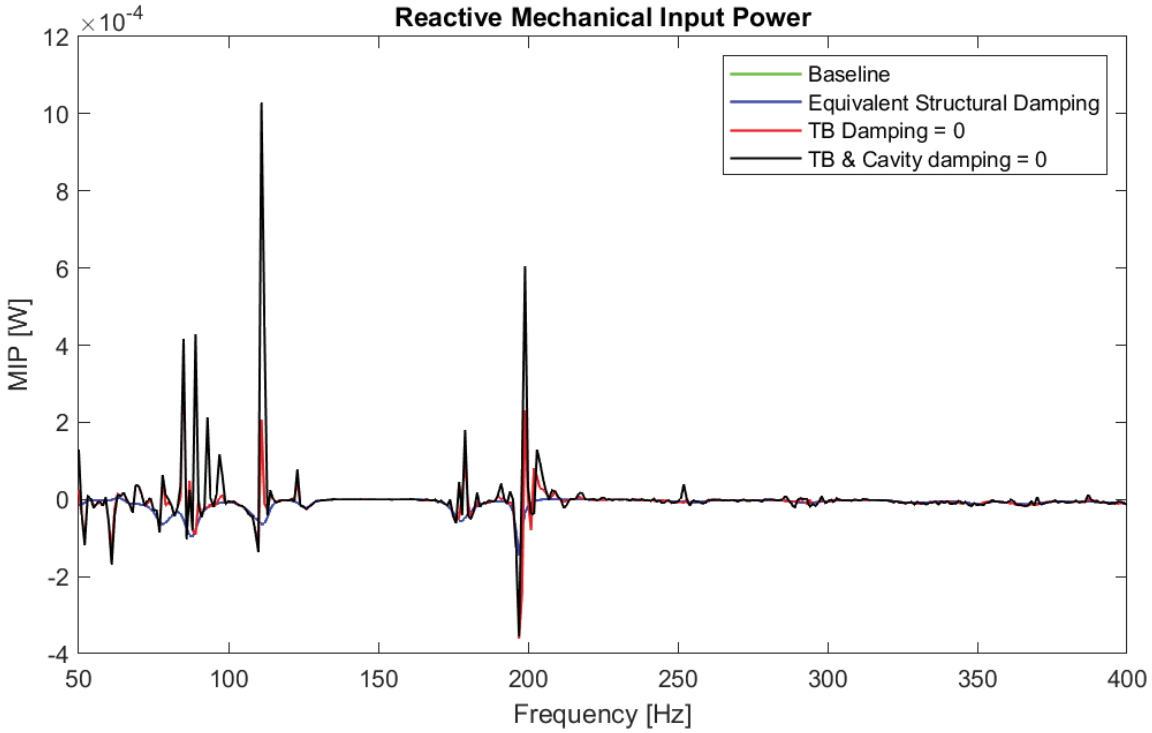

Figure 5.22: Reactive MIP for all 4 experiments

Reactive power results obtained in Figure 5.22 show expected behaviour, that is the reactive power increases with a decrease in damping within system. This happens because of undamped vibrations and standing waves produced. A large peak at 112 Hz is obtained which suggests the resonant frequency of cavity fluid is at 112 Hz.

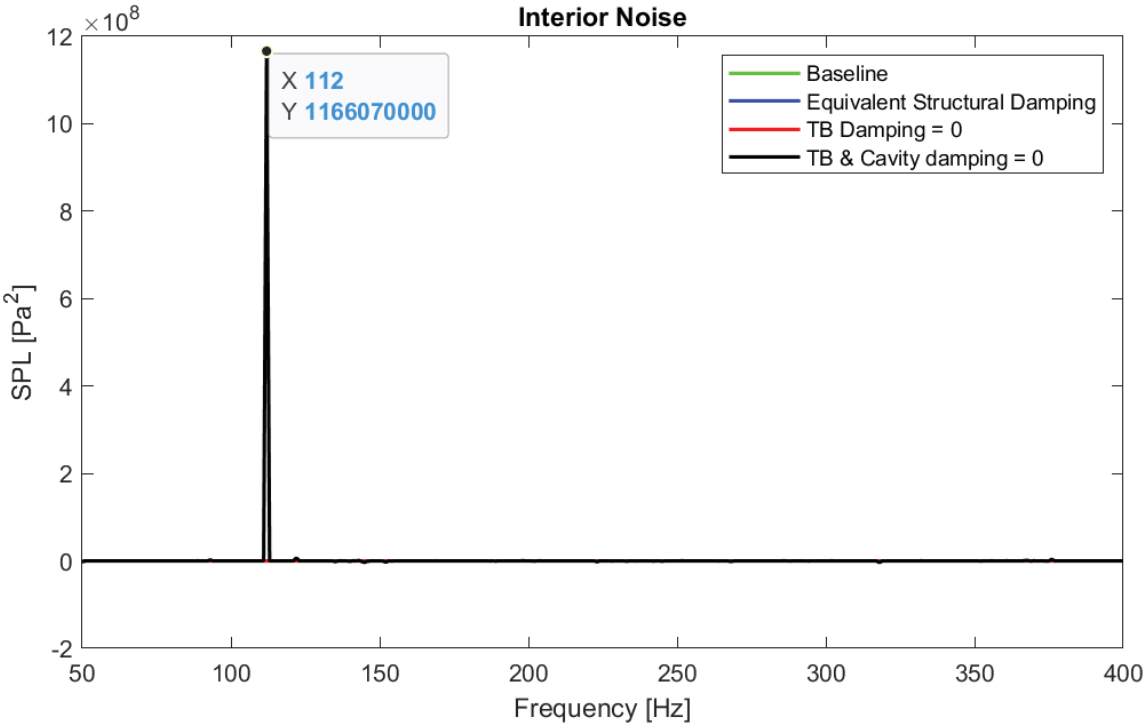

Figure 5.23: SPL for all 4 experiments

Figure 5.23, 5.24 and 5.25 show the SPLs obtained for all experiments. SPL obtained for first two experiments is the same as observed in previous sections, of the order of $2*10^{-2}$ Pa. Whereas for zero trimmed body damping, interior noise is of the order of 10^3 to 10^4 Pa, and increases to the order of 10^4 to 10^8 Pa as the cavity damping is also reduced to zero with a distinct peak at 112 Hz. This behaviour is quite intuitive, for decreasing damping within system. However, it also shows that without cavity damping, reactive power has better correlation to SPL. The recurring large peak for noise and reactive power at 112 Hz confirms a good correlation between them for no cavity damping, and also shows that the natural frequency of cavity fluid is at this frequency.

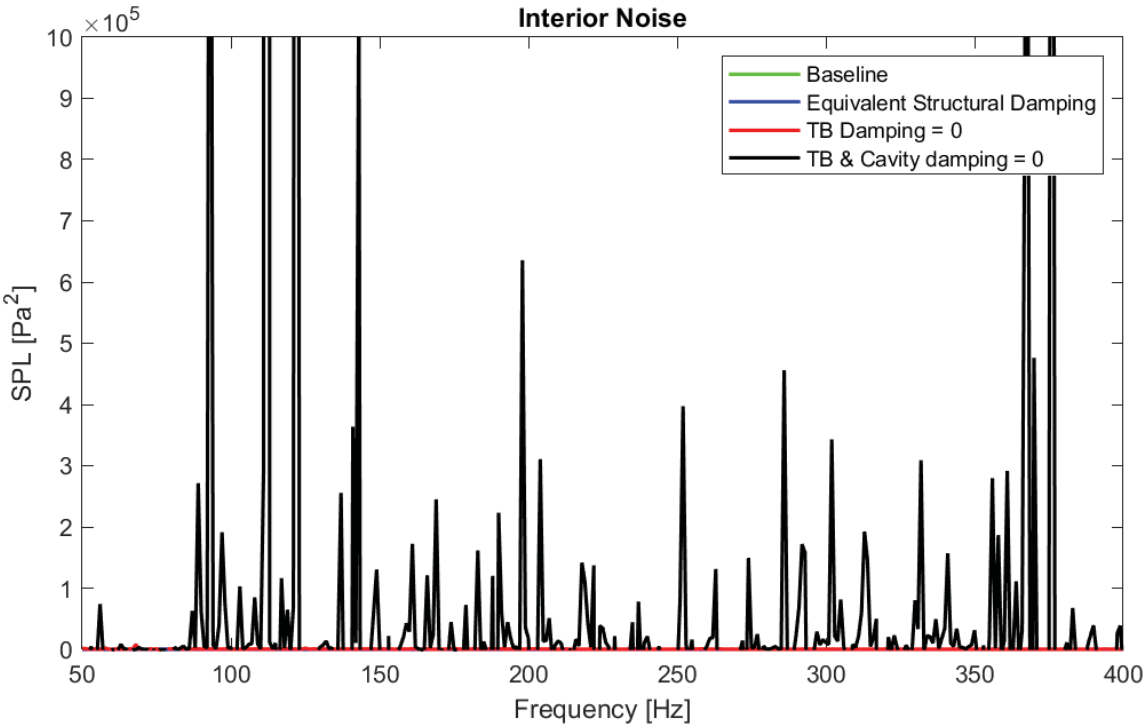

Figure 5.24: SPL for all 4 experiments

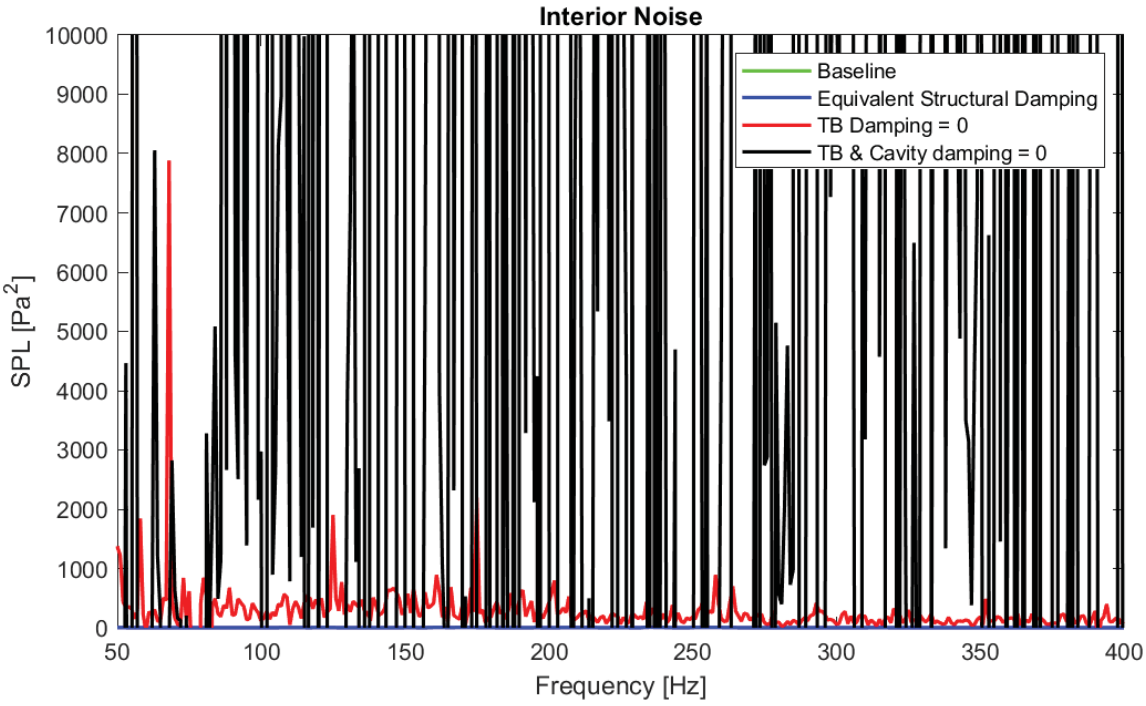

Figure 5.25: SPL for all 4 experiments

Because of relatively low active powers and extremely high interior noise obtained for experiment 3 and 4, the transfer function $T_{active}(f)$ also shows a similar behaviour to SPLs as can be seen in Figure 5.26, 5.27 and 5.28.

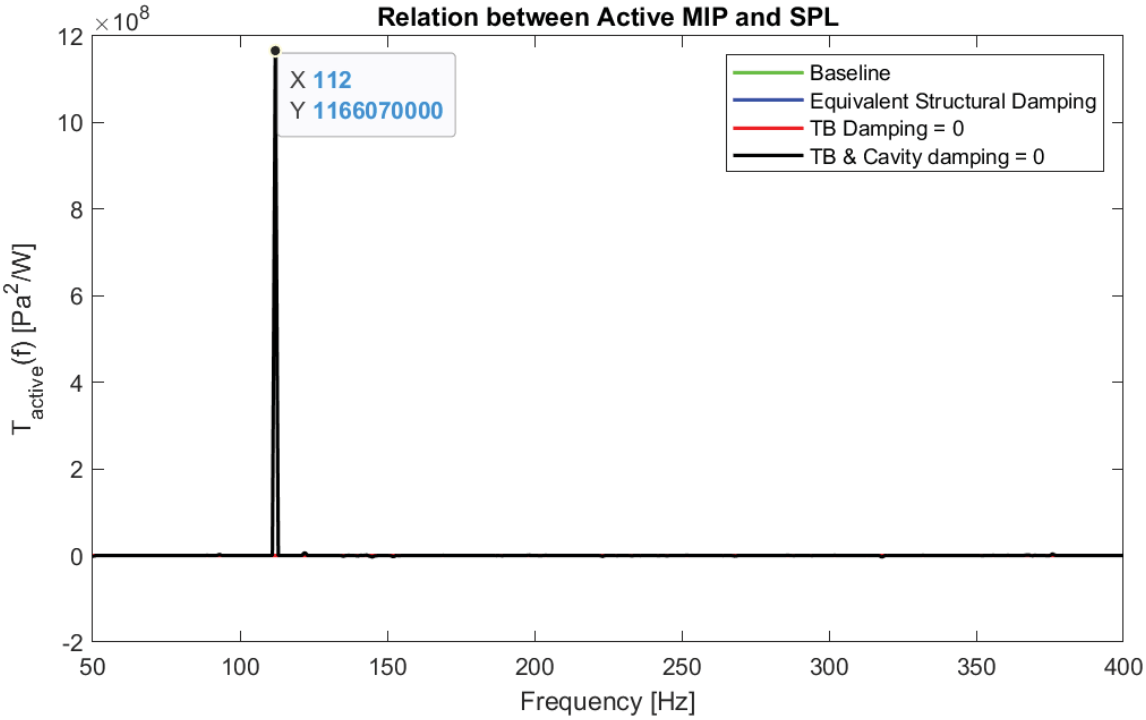

Figure 5.26: T(f) for Active power and SPL

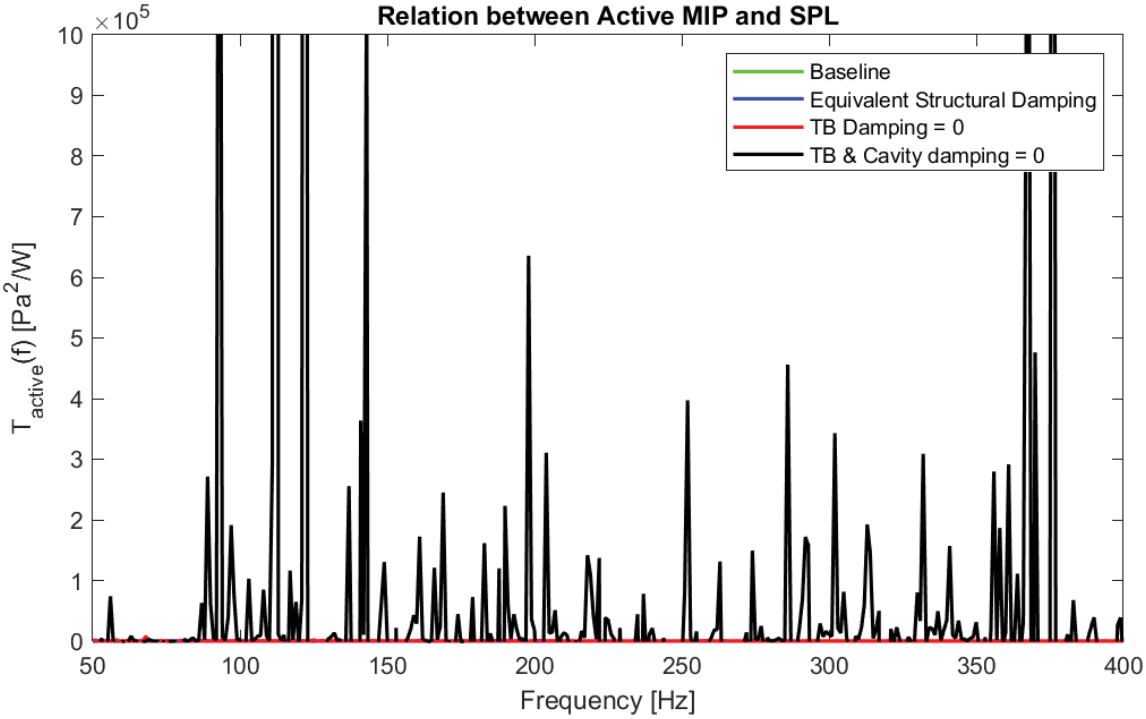

Figure 5.27: T(f) for Active power and SPL

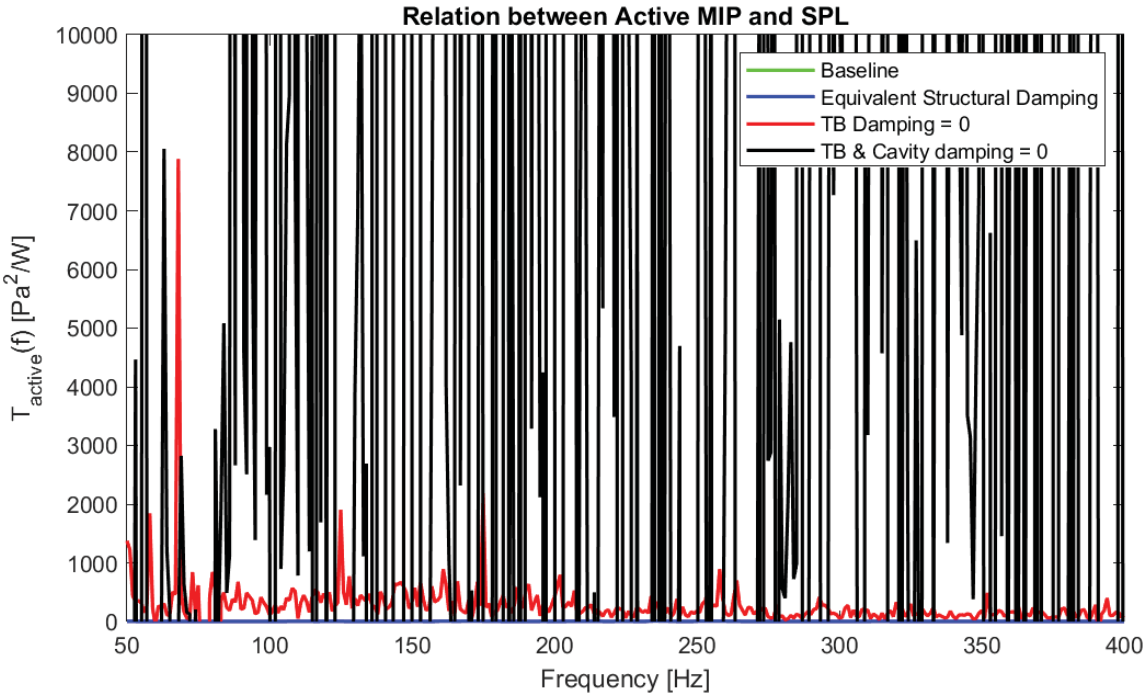

Figure 5.28: T(f) for Active power and SPL

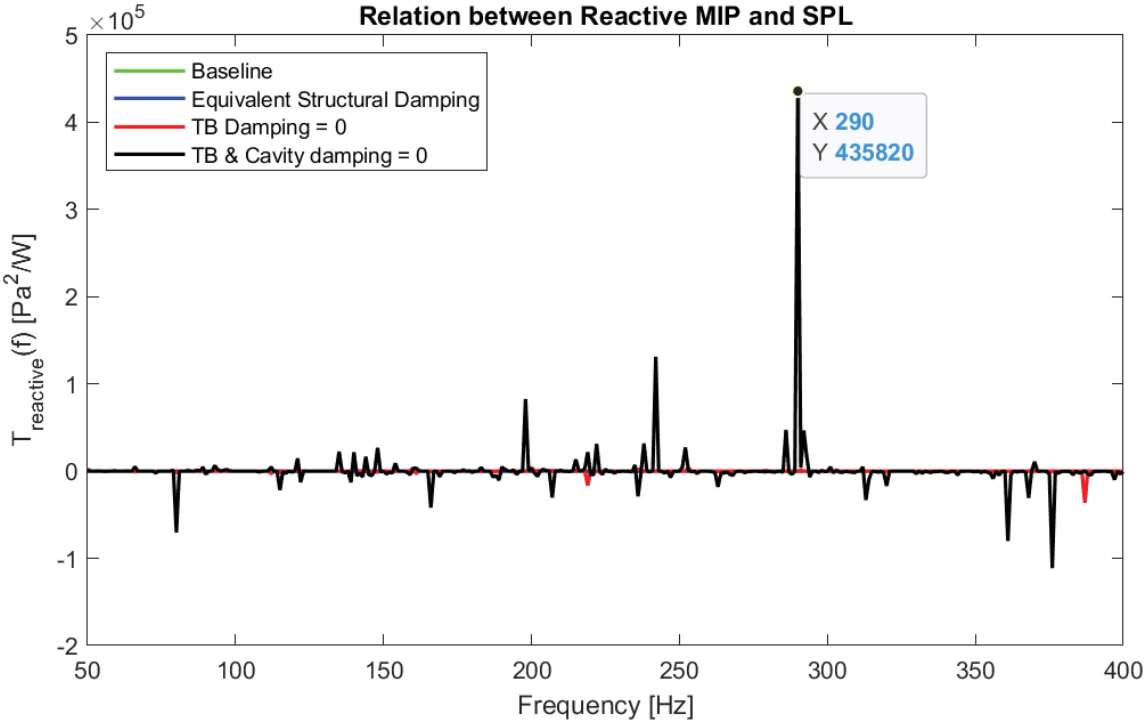

Figure 5.29: T(f) for Reactive power and SPL

However, in the case of relation between reactive MIP and SPL as shown in Figure 5.29 and 5.30, although still a poor correlation, reactive MIP correlates better than active MIP to the interior noise.

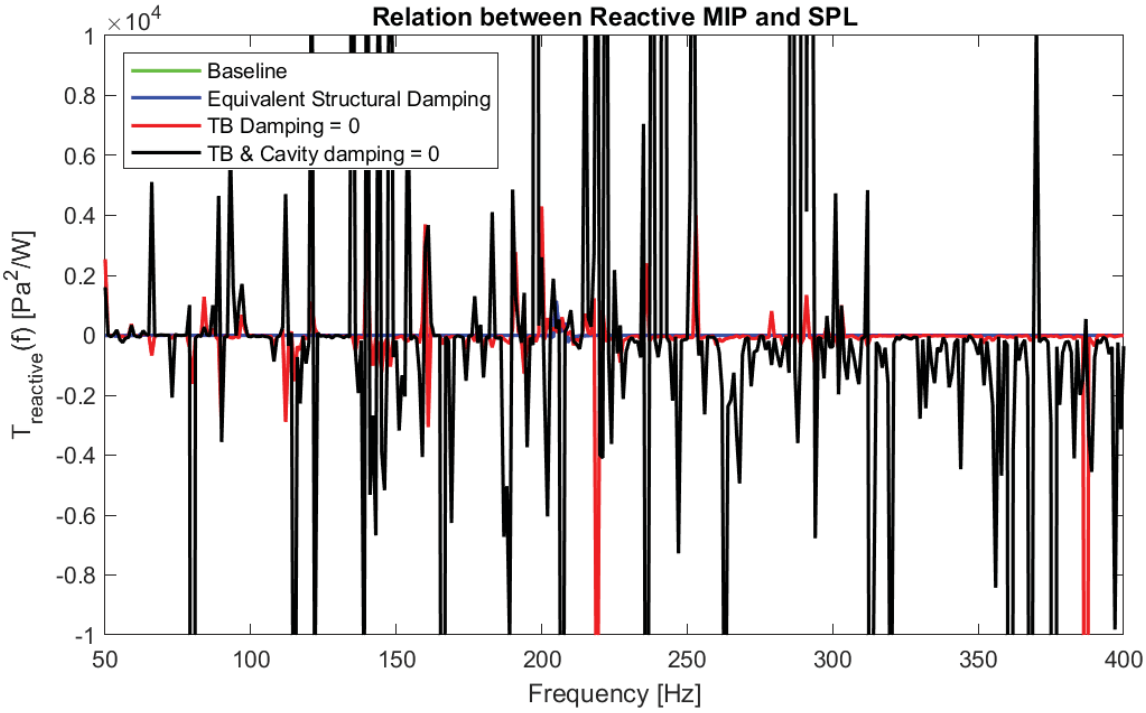

Figure 5.30: T(f) for Reactive power and SPL

In conclusion, body and cavity damping show a huge impact on the active/reactive MIP as well as SPL. The correlation between SPL and active MIP appears to starts deteriorating as damping is reduced within trimmed body. Whereas, an opposite effect is observed for reactive MIP and SPL relation. But, if in addition to trimmed body the cavity fluid damping is also put to zero, a similar impact is obtained but in much greater magnitude. That is, SPL starts to correlate much better with reactive MIP, whereas, active MIP seems to lose any connection to SPL.

Chapter 6

Discussion

Limited knowledge of damping and its modelling within parts of a vehicle body has led to subpar enhancement of its vibro-acoustic properties. This has long restricted the expected addition to vehicle design from NVH perspective, that is planned for early phases of vehicle development programs. This is the central problem that the research has aimed to take first steps towards.

Results obtained indicate that although values of MIP and SPL reduced with increasing damping values within suspension (Figure 5.14 and 5.15), impact on the measure of their correlation or T(f) was not so straight forward (Figure 5.16). Localization of structural damping into connectors provided the most uniform T(f) and hence the best correlation among measured cases, with an increasingly improved correlation for higher damping value. Contrary to this, equivalent viscous damping localized into connectors or structural damping localized into components displayed a poorer correlation that deteriorated with increasing damping value. Since, it is connectors where the actual dissipation of energy takes place, localization of structural damping into connectors (out of all damping cases) has shown to capture the effect of damping better.

The data of comparison between active and reactive mechanical input power suggests a strong correlation between active power and interior road noise for most damping cases other than where damping in trimmed body and/or cavity is put to zero, in which case, reactive mechanical input power takes an upper hand in correlating with interior noise. The correlation between both seems to improve drastically with decreasing damping withing trimmed body and cavity. The values of both (reactive power and noise) jump up to very high magnitudes and this behaviour indicates a disparity in actual belief, that active power is the only cause of interior noise.

These results build on existing evidence of good correlation between mechanical input power and interior road noise, and add a layer of knowledge about damping to NVH CAE procedures. These however, do not fit completely with the claims of active power being the sole source of interior noise and it is beyond the scope of this study to compare or dive further into active and reactive power contribution.

Chapter 7

Conclusions and Future Work

The dissertation raises questions on reliability of damping models used for NVH CAE studies during early development phases of vehicle development programs, and takes the first steps in investigating how different damping models impact system behaviour. Understanding the role of damping in using mechanical input power as an indicator for estimating interior noise has been the final goal of this research direction. This dissertation has aimed to achieve that by studying impact of different modelling of damping within the suspension, on the power input to trimmed body, interior road noise produced and the relation between them.

The methodology started off defining the scope of research to the most relevant transfer paths within calculation model and frequency ranges they are major contributors in. This was followed by defining a mathematical relation between MIP and SPL (T(f)) and also a measure of the quality of their correlation (standard deviation of T(f)).

In expectation to find out answers to damping effects, the methodology so chosen turned out to yield straightforward and robust results, while providing new insights into the limitations of this research which are discussed further in this section. For instance, changing damping within suspension showed a meagre impact on dynamic behaviour of system even after increasing 5 times the damping values within suspension, and this has led to the research pointing towards role of other dynamic effects within the suspension or trimmed body, etc., in the process of energy transfer from wheels to body. Similarly, though there have been studies in the past aiming at correlating body input power and interior noise levels, they have restricted their study to studying relation between active power and SPL (based on theoretical results) and deemed reactive power as irrelevant to the study. This research provides a basis to direct future studies in investigating further the role of complex mechanical input power (active + reactive power) in producing interior road noise.

The dissertation is directed towards conceptualizing a new way of estimating interior road noise for a vehicle during concept phases at Volvo Cars, by considering power as an indicator for road noise (owing to its exceptionally good correlation with interior sound pressure levels) and it has taken a first step in this direction and provided a background to continue the work further by conducting in depth research studies on the dynamic behaviour of vehicle body and addressed gaps within available research projects that did not explicitly involve impact of damping parameters on the system behaviour. Furthermore, based on these conclusions, future studies should consider validating the results of simulation model by conducting physical tests on actual vehicles and include concrete evidence for choosing active power for analysis

among others.

This has led to a conclusion that localization of structural damping into connectors could be a better modelling technique to capture damping within suspension, and physical tests can be conducted to validate these claims.

Although a conclusion has been drawn in favour of active power, a correlation between interior noise and reactive power that improves with decreasing damping within trimmed body and cavity, arises questions on role of active power being the sole contributor to production of interior noise. This also results in a suggested future work to check the correlation between SPL and magnitude of complex power for more concrete conclusions.

These behaviours suggest a very complex dynamic relation between the trimmed body, suspension and its components, wheel assembly, and cavity fluid. To develop better understanding of the system, it is recommended to include their study into future work, and check if it indeed it is majorly suspension or other components that are related to interior noise reduction.

Bibliography

[1] *Fundamental Mechanics*. John Wiley Sons, Ltd, ch. 5, pp. 87–117. [Online]. Available: https://onlinelibrary.wiley.com/doi/abs/10.1002/9780470978160.ch5

[2] L. Gagliardini and A. Gaudin, "Recent improvements in road noise control," 05 2007.

[3] S. Hambric, "Power flow and mechanical intensity calculations in structural finite element analysis," *Journal of Vibration and Acoustics*, vol. 112, 10 1990.

[4] A. Jund and L. Gagliardini, "Noise control using input power at low and mid-frequencies: sensitivity to structural design changes," 09 2010.

[5] C.-C. Liu, F. Li, L. Tang, and W. Huang, "Vibration control of the finite l-shaped beam structures based on the active and reactive power flow," *Science China: Physics, Mechanics and Astronomy*, vol. 54, pp. 310–319, 02 2010.

[6] N. S. Ottosen and M. Ristinmaa, "3 - stress tensor," in *The Mechanics of Constitutive Modeling*, N. S. Ottosen and M. Ristinmaa, Eds. Oxford: Elsevier Science Ltd, 2005, pp. 49–65. [Online]. Available: https://www.sciencedirect.com/science/article/pii/B9780080446066500035

[7] P. Persson, O. Flodén, and B. Pedersen, "Predicting vibroacoustic performance of thin-walled lightweight structures during conceptual design," *Finite Elements in Analysis and Design*, vol. 169, p. 103342, 2020. [Online]. Available: https://www.sciencedirect.com/science/article/pii/S0168874X1930352X

[8] S. Sicklinger and R. Ullmann, "Structural power as an acoustic design criterion for the early phase of product design," 09 2018.

[9] R. Ullmann, S. Sicklinger, M. Buchschmid, and G. Müller, "Power-based approach for assessment of structure-borne sound in mechanical networks of vehicle structures," *Procedia Engineering*, vol. 199, pp. 1386–1391, 2017, x International Conference on Structural Dynamics, EURODYN 2017. [Online]. Available: https://www.sciencedirect.com/science/article/pii/S1877705817338614

Faculty of Engineering, Blekinge Institute of Technology, 371 79 Karlskrona, Sweden